Title

Targeted Polymeric Micelles for Anti-inflammatory Drugs for Ocular Application

Author

Gu, Yimin

Publication Date

2023

Peer reviewed|Thesis/dissertation

UNIVERSITY OF CALIFORNIA

Los Angeles

Targeted Polymeric Micelles for Anti-inflammatory Drugs for Ocular Application

A thesis submitted with partial satisfaction

of the requirements for the degree Master of Science

in Chemical Engineering

by

Yimin Gu

2023

ABSTRACT OF THE THESIS

Targeted Polymeric Micelles for Anti-inflammatory Drugs for Ocular Application

by

Yimin Gu

Master of Science in Chemical Engineering

University of California, Los Angeles, 2023

Professor Nasim Annabi, Chair

Inflammation is one of the most common conditions that impact the health of the eye. Due to the static and dynamic barriers caused by the tear film and blinking, effective and sustained delivery of anti-inflammatory pharmaceutics remains a challenge of ocular treatment. Surface functionalization with mucoadhesion moieties on drug slivery systems could boost the bioavailability of pharmaceutics by increasing the retention time on corneal mucin. Herein, in chapter I, we developed a polymeric micelle (MC) as a nano-drug carrier and functionalized it with an ocular-targeted moiety, phenylboronic acid (PBA). The MC is composed of poly (ethylene glycol)-b-poly(N-(2-hydroxypropyl) methacrylamide-oligolactate) (PEG-b-(HPMA-Lac_{m+1})) copolymers. The HPMA-Lac_{m+1} was modified to increase the encapsulation efficiency (EE%) for anti-inflammatory drugs. The EE% of loteprednol etabonate (LE) was increased by more than 20% compared to the result prior to the modification in this study and to a previous work published by our lab.[1] The resulting MC exhibited a sustained release profile of LE for 12 days. PBA functionalization achieved a 91.5% conjugation efficiency on the PEG, and the resulting PBA-MC exhibited excellent adhesion to mucin. Further, high cell viability (>95%), cell spreading, and

proliferation of human corneal epithelial cells was found after incubation with PBA-MC for five days. Therefore, PBA-MC is a promising candidate for delivering the anti-inflammatory drug (LE) to the ocular target. In addition, the MC was synthesized using PEG with an amine chemical handle, which allows for further functionalization of various moieties. For example, in chapter II, gallic acid (GA) was conjugated onto PEG through the amine group as an alternative mucoadhesive moiety. Further, PEG provides numerous sites for hydrogen interactions. In chapter III, tannic acid (TA), another outstanding mucoadhesive group, was crosslinked onto the surface of MC through hydrogen bonding with PEG. However, the incorporation density of GA and TA was suboptimal in this study and require further optimization.

The thesis of Yimin Gu is approved.

Junyoung O. Park

Panagiotis D. Christofides

Nasim Annabi, Committee Chair

University of California, Los Angeles

2023

List of abbreviations used in this thesis:

^{1}H NMR: hydrogen-1 nuclear magnetic resonance

ACN: Acetonitrile

ACVA: 4,4′-Azobis(4-cyanovaleric) acid

$CDCl_3$: deuterated chloroform

$(CD_3)_2SO$: deuterated dimethyl sulfoxide

DCC: N,N'-Dicyclohexylcarbodiimide

DCM: methylene chloride

DMF: dimethylformamide

DMSO: dimethyl sulfoxide

DP: 4-dimethylamino pyridinal

EDC: 1-Ethyl-3-(3-dimethylaminopropyl)carbodiimide

HPMA: N-(2-hydroxypropyl)methacrylamide

PEG-*b*-(HPMA-Lac_{m+1}): poly (ethylene glycol)-poly(N-(2-hydroxypropyl)methacrylamide-lactate)

GA: gallic acid

Lac: lactide

LE: loteprednol etabonate

L-lactide : (3S)-cis-3,6-dimethyl-1,4-dioxane-2,5-dione

MC: micelle

NHS: N-Hydroxysuccinimide

NMR: nuclear magnetic resonance

PBA: 4-carboxyl phenylboronic acid

PBS: phosphate buffered saline

PEG: polyethylene glycol

$Sn(Oct)_2$: $Tin(II)_2$ ethylhexanoate

TA: tannic acid

TEA: triethylamine

THF: tetrahydrofuran

TFA: trifluoroacetic acid

TLC: thin layer chromatography

TS: p-toluensulfonic acid

Table of Contents

List of figures

Acknowledgments

I would like to sincerely thank my advisor Dr. Nasim Annabi for giving me the opportunitsy to learn and explore drug delivery research as a Master's student in her lab. Throughout my Master's journey, she gave me great guidance, support, and encouragement. I would like to thank my mentors--Yuting Zheng and Yavuz Oz. This project would not have been done without them patiently training me with laboratory techniques and teaching me the skills of analysis and troubleshooting in the first place. Thanks to Ronak Afshari, our lab manager and postdoctoral research scholar, for sharing much of her advice in the chemistry field and helping me with lab material inventory and paperwork for working in this lab. I would like to thank Dr. Martin Phillips, Ivo Atanasov, Jane Yang, Dr. Kanji Niwa, Joyce Huang, Dr. George Aninwene II, and many members of the Chemistry Department, California NanoSystems Institute, Engineering Department, and David Geffen School of Medicine. They provided generous help for my training and allowed me to conduct experiments in their departments and laboratories. Thanks to all my lab colleagues who have constantly been helping me with ideas, brainstorming, troubleshooting, and presentation practice. Lastly, I would like to thank Professor Junyoung Park and Professor Panagiotis Christofides for being my Master's thesis committee. None of these would have been possible without your support.

Introduction

Inflammation in the eye is a common condition typically treated using conventional methods, such as topical eye drops and ointments. However, these methods have limitations in effectively delivering drugs to the intraocular tissues. The limitations are primarily due to the static and dynamic ocular barriers that impede the uptake of topically applied drugs. While these barriers are crucial in protecting the eyes from environmental stress, they also hinder the delivery and retention of conventional topical drug molecules on the cornea. In addition to ocular barriers, many anti-inflammatory drugs are hydrophobic, further reducing their bioavailability in the eye. When administered topically, these drugs often have less than 5% bioavailability at the intended target site, primarily due to the aforementioned barriers.[2, 3] Consequently, frequent application of the drugs is necessary to achieve the therapeutic dosage required for effective treatment against inflammation. To address these challenges, novel ocular delivery systems have been developed as alternatives to the current treatment methods. These systems include nanoparticles (NPs),[4] microneedles,[5, 6] drug-eluting contact lenses,[7, 8] and polymeric micelles (MCs).[9] The primary objective of these delivery systems is to prolong the retention time of anti-inflammatory drugs on the ocular surface, thereby increasing the chances of reaching the intraocular tissues. By utilizing these advanced delivery systems, the bioavailability of anti-inflammatory drugs can be significantly improved. They help overcome the limitations posed by ocular barriers and hydrophobic drug properties, enabling enhanced drug delivery to the targeted sites within the eye. This advancement in drug delivery technology offers promising prospects for more effective treatment of ocular inflammation.

In the past few decades, polymeric MCs have emerged as a superior choice among various delivery systems due to their advantageous features, including high drug encapsulation efficiency and controlled drug release capabilities.[10] These MCs are formed through the self-assembly of amphiphilic polymers in an aqueous environment, allowing them to efficiently encapsulate hydrophobic drug molecules within their cores and enhance the solubility of these medications. This property makes them particularly suitable for delivering hydrophobic drugs.[11] Despite their effectiveness in encapsulating hydrophobic drugs, MCs face a challenge regarding their rapid clearance from the ocular surface due to factors such as constant blinking and tear flux. To overcome this limitation and achieve active targeting of the ocular surface, surface modification of polymeric MCs with a suitable targeting group is necessary. Commonly employed targeting moieties include PBA,[3, 12-15] maleimide,[16-23] and thiol groups.[24, 25] Among these functional groups, PBA stands out as a promising candidate for mucosal targeting because it can covalently bind to sialic acid groups found in mucin. By incorporating PBA groups on the surface of micellar delivery systems, the issue of rapid clearance can be addressed, leading to extended retention on the ocular surface. This surface modification enables the MCs to actively target the ocular tissues and enhance drug delivery to the interior parts of the eye.

In order to overcome the challenge of retention time on the cornea, this work focuses on forming covalent interactions between the micellar drug delivery system and the targeted site. The MC is formed by a copolymer poly (ethylene glycol)-block-poly (N-(2-hydroxypropyl) methacrylamide-lactate) (PEG-b-(HPMA-Lac_{m+1})). In chapter I, PBA was conjugated onto the MC, and the conjugation was optimized to ensure high efficiency that would increase the retention time of MC on the ocular surface. Moreover, in chapter II,

gallic acid (GA) was examined as a potential alternative to PBA. In chapter III, tannic acid (TA) was incorporated onto PBA-MC as an attempt to improve mucoadhesion.

Chapter I. Targeting MCs through PBA functionalization

1.1 Introduction

Drug delivery for ocular diseases faces challenges of retention of the therapeutics.[13] Ointments, hydrogels, adhesive patches, drug-eluting soft contact lenses, and ocular inserts are common approaches to increase the retention time of therapeutics.[26, 27] However, the ocular surface is a sensitive area; solid gels, patches, and inserts containing therapeutics can adhere to the ocular surface, but they often cause discomfort and technical barriers for the patients to apply them properly. Eye drops can be easily applied; however, due to the blinking force from the eyelids and the fast turnover rate caused by the tear, eye drops are frequently rinsed away and usually require multiple administrations on a daily basis, which significantly lowers the patients' compliance.

In order to improve the retention of the drugs on the cornea, targeted nanocarriers emerged as a new approach. Nanocarriers can be easily loaded into an eye drops formulation. These targeted nanocarriers often contain moieties that can form strong interactions, such as covalent bonds, with the ocular surface.[28-31] Such moieties would allow highly selective targeting in ambient conditions. The covalent bonds greatly boost the retention time of the drug carriers on the cornea, allowing the carrier to slowly degrade near the target, significantly improving the bioavailability of the encapsulated drugs for ocular diseases. Examples of the targeting moieties include PBA,[3, 12-15] maleimide,[16-23] and thiol groups.[24, 25] Due to its unstable nature, using maleimide often needs protection groups to prevent it from degrading during multi-step synthesis.[32] Thiol groups are prone to oxidization, and the resulting linkages between the thiol groups and the targets are often reversible.[33] On the other hand, PBA can form covalent bonds with the cis-diol group-containing compounds, including polysaccharides, glycoproteins, and glycolipids.[12, 15] This interaction leads

to the formation of boronic esters that are stable at physiological pH.[34] Due to this property, numerous studies have taken advantage of the carbohydrate-targeting nature of PBA. For example, micellar nanocarriers have been previously functionalized with PBA to target glycan-rich mucin layers in the eyes,[3, 12] sialic acid-overexpressed cancerous cells,[35-37] and to release encapsulated insulin upon hyperglycemia detection.[38] In recent years, PBA has gained an increasing amount of spotlight on ocular applications because of its ability to react with the diol groups on the glycoprotein and glycolipids on the corneal mucin. Studies reported outstanding treatment effects using PBA-functionalized nano-drug carriers for eye diseases.[12, 15] A list of the ocular-targeting nanocarrier using PBA is summarized in Table 1. Some studies achieved good *in vitro* and *in vivo* ocular-targeting outcomes due to PBA grafting.[15] However, these studies share common drawbacks, including low PBA conjugation efficiency and an initial burst release of the drugs. In this chapter, PBA was selected as a targeted moiety due to its stable interaction with mucin. To address the current limitation of PBA functionalized nano-delivery systems, I specifically investigated improving conjugation efficiency to enhance the targeting effects

Table 1. PBA-functionalized nanocarrier for ocular applications

Material Design	PBA conjugation efficiency	Drug and encapsulation efficiency	Release Profile	Outcome	Ref.
PBA-chitosan oligosaccharide-vitamin E MC	15.4%	coumarin-6 85.0 ± 0.4%	75% was released at 0.5 h and almost all drugs were released at 2 h	PBA group yielded lower amount of fungal colony-forming units (0.09 fold) than the control *in vivo*	[15]
PBA-poly(Lac)-dextran NP	17.6 % ± 2.7%	cyclosporine A 11.9 ± 1.6 wt%	released for 5 days; near 40% was released at 12 h and over 50% by day 1	Released clinically relevant dosage for 5 days	[4]
poly(Lac)-b-poly(methacrylic	20 wt%	cyclosporine A 15 wt%	35 to 45% released by day 1, 74 to	Reduced the initial burst release	[3]

acid-co-PBA) MC			80% after 14 days	Showed reduced cell proliferation and altered morphology	
Poly(Lac)-b-poly (methacrylic acid-co-3-acrylamido-PBA) MC	/	latanoprost 23.7 ± 1.2%	80% was released after 12 days	Reduced intra-ocular pressure *in vivo* more than the control	[112]
(3-aminomethyl PBA)-conjugated chondroitin sulfate nano-lipid carrier	4.7 ± 0.8%	dexamethasone 88 ± 2%	25% was released at 1 h, ~90% by 12 h	High drug encapsulation efficiency Not a carrier for sustained release	[12]
PBA-methylcellulose-poly(N-tert-butylacrylamide) MC	/	dexamethasone 95%	~2-11% was released by day 1, depending on the degree of hydrophobic modification	Drug-loading efficiency can be tuned by grafting the density of hydrophobic moieties	[39, 40]

Prior to PBA functionalization, I first modified a polymeric MC that was previously developed[1, 41] as a micellar drug delivery platform. This MC was formed by PEG-*b*-(HPMA-Lac_{m+1}) block copolymer. The hydrophilic shell was made of PEG chains, a material widely used as a biocompatible polymer, due to its prolonged lifespan in circulation and low risk of triggering immune responses.[42, 43] The hydrophobic core was made of *b*-(HPMA-Lac_{m+1}); it can encapsulate non-water-soluble drugs and is biodegradable through hydrolysis of the ester bonds.[1, 44]

The monomer of the HPMA-Lac_{m+1} block was obtained via a ring-opening polymerization (ROP) between HPMA and L-lactide catalyzed by $Sn(Oct)_2$, as previously reported.[1, 44] This synthesis method yielded a mixture of HPMA-Lac_{m+1} (m = 1, 3, 5). As the monomers were used to synthesize amphiphilic copolymers, different numbers of Lac repeating units contributed to various hydrophobic chain lengths of the copolymer. MCs synthesized using longer hydrophobic chains

resulted in lower cloud points,[45] larger sizes, lower critical micelle temperatures, and lower critical micelle concentrations (CMC).[41] A low CMC is desirable for drug delivery. The concentration of MCs can be diluted after entering the human body. Failing to maintain CMC would cause MC to disassemble prematurely. Efforts have been made to reduce CMC, including co-injecting non-drug-loaded MC to raise micelle concentration,[46-48] modifying the hydrophobic segment of the polymer backbone, and incorporating amphiphilic surfactants to lower the CMC due to synergistic interactions.[49] In addition, studies using nanoparticles as drug delivery platforms reported that the encapsulation efficiency of non-polar drugs increased by increasing the ratio of hydrophobic: hydrophilic building blocks.[50, 51] However, an insufficient amount of studies demonstrated whether increasing the hydrophobic chain lengths of the MC copolymer can lead to better encapsulation of non-polar drugs. Therefore, I first focused on purifying monomers with various hydrophobic chain lengths. These purified monomers were used to synthesize MCs to assess the encapsulation efficiency of LE. Then, PBA was incorporated into the MC to improve the retention of the micellar drug carrier on the cornea. PBA can form covalent interaction with sialic acid and other structures with cis-diol on corneal mucin.[12, 15] A schematic illustration of PBA-functionalized MCs and how it interacts with the cornea is shown in Figure 1.

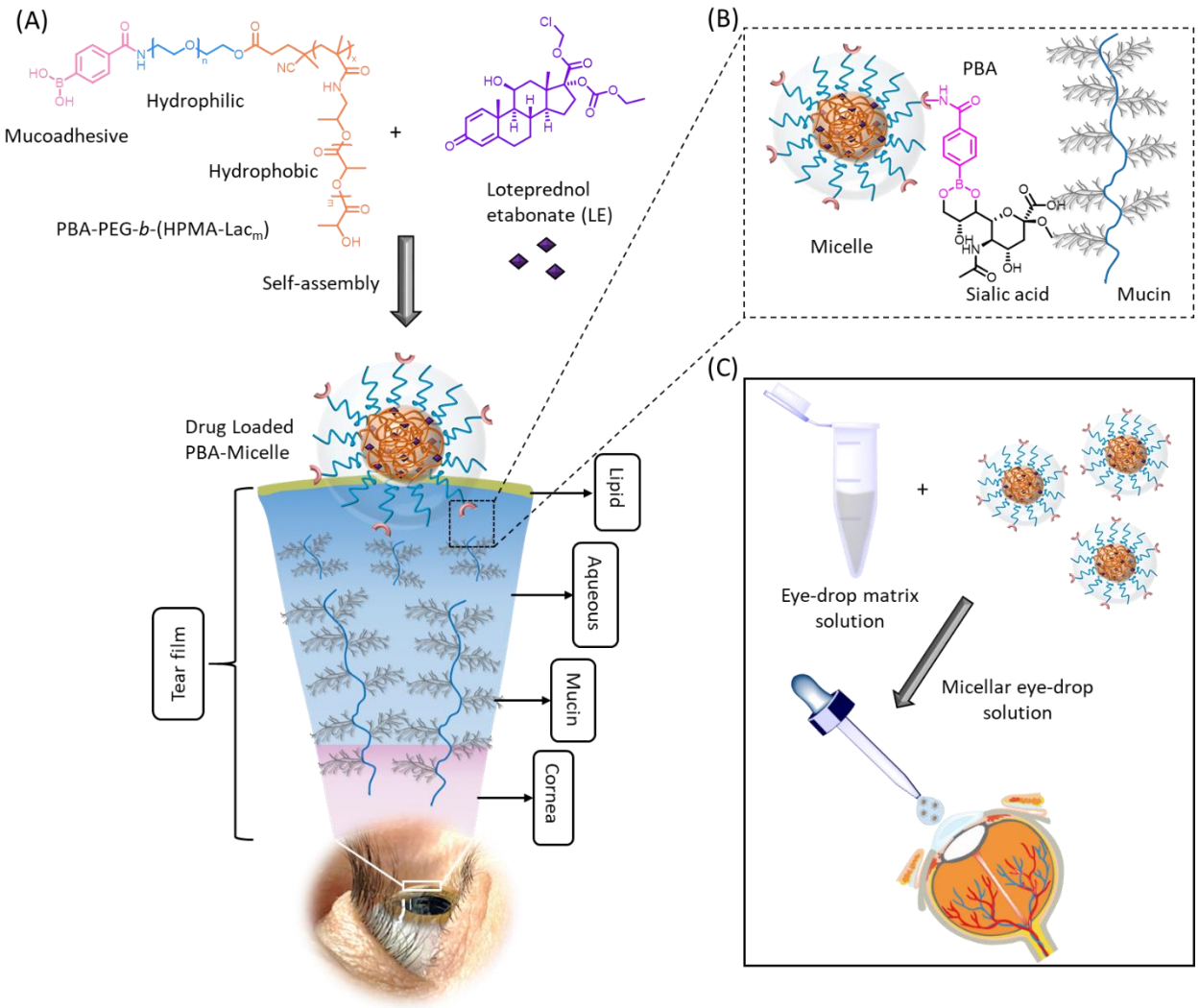

Figure 1. (A) Formation of LE-loaded MCs with PBA-PEG-*b*-(HPMA-Lac_{m+1}) copolymer in a buffer solution. PBA-PEG-*b*-(HPMA-Lac_{m+1}) copolymer self-assembled into MC structure in an aqueous environment; (B) schematic illustration of the interaction between LE loaded PBA-MCs and sialic acid groups of mucin on the ocular surface; (C) dispersion of MCs in an eye-drop solution for the release of LE from micelles in a targeted manner.

1. 2 Materials and methods

1.2.1 Materials

Tert-butyloxycarbonyl (tBoc) protected amine polyethylene glycol (tBoc-NH-PEG-OH, MW 3.4k) was purchased from Biopharma PEG Scientific Inc.. 4-carboxyl phenylboronic acid (PBA), (3S)-cis-3,6-dimethyl-1,4-dioxane-2,5-dione (L-lactide) were purchased from Sigma-Aldrich. N-(2-hydroxypropyl)methacrylamide (HPMA) was purchased from Polysciences, Inc. 4-methoxyphenol was purchased form Acros Organics Chemicals, Thermo Fisher. 1-Ethyl-3-(3-dimethylaminopropyl)carbodiimide (EDC), N,N'-Dicyclohexylcarbodiimide (DCC), and N-Hydroxysuccinimide (NHS) were purchased from Tokyo Chemical Industry Co., Ltd. (TCI Chemicals). 4,4′-Azobis(4-cyanovaleric acid) (ACVA), 4-dimethylamino pyridinal (DP), p-toluensulfonic acid (TS), Tin(II2 ethylhexanoate ($Sn(Oct)_2$), porcine gastric mucin were purchased from Sigma. Acetonitrile (ACN), ethyl acetate, hexane, cyclohexane, tetrahydrofuran (THF), ethanol, methanol, dimethyl sulfoxide (DMSO), methylene chloride (DCM), trifluoroacetic acid (TFA), deuterated chloroform ($CDCl_3$), and deuterated dimethyl sulfoxide ($(CD_3)_2SO$) were purchased from UCLA chemical store. Human corneal epithelial cells (PCS-700-010) were purchared from American Type Culture Collection. Alveolar epithelial cell medium was purchared from ScienCell. Live/Dead^{TM} Viability/Cytotoxicity Kit, Alexa Fluor 594−phalloidin, and DAPI were purchased from Invitrogen.

1.2.2 Synthesis of MCs

1.2.2.1 Synthesis of NH_2-PEG and PBA-PEG

The protection group of tBoc-NH-PEG-OH (200 mg, 58 μmol) was cleaved by a 1:1 (v/v) mixture of TFA (1 mL) and DCM (1 mL). The mixture was shaken at 130 rpm in a shaker at 25 ºC for 4 hours to deprotect the primary amine group. After the deprotection reaction, NH_2-PEG was diluted

by DCM, followed by evaporation using a rotary evaporator and dialysis against Mili-Q water. Then, NH_2-PEG (105 mg, 0.2 equivalent) solution was prepared in 0.8 mL 0.1M MES buffer at pH = 6. Separately, EDC (148 mg, 5 equivalent) dissolved in 0.1 mL MES buffer was added to PBA (25.5 mg, 1 equivalent) dissolved in 0.1 mL DMSO. This mixture was stirred at 45 °C for 20 min, followed by dropwise addition of NHS (35.5 mg, 2 equivalent) dissolved in 0.1 mL MES buffer). Then, the mixture was stirred at 45 °C for 2 hours to activate the carboxyl functional group on PBA. Finally, the NH_2-PEG solution was added dropwise to this mixture, and the pH was adjusted to 7 using NaOH. The reaction was allowed to proceed for 20 hours. The product was purified by dialyzing against Mili-Q water for 5 days, and obtained by freeze-drying.

1.2.2.2 Synthesis of monomer HPMA-Lac_{m+1}

The monomer was synthesized using HPMA and L-lactide. The resulting products contain multiple lactide repeating units —[$COCH(CH_3)O$]— and a —$COCH(CH_3)OH$ tail. m denotes the total number of repeating units. The monomer was named HPMA-Lac_{m+1}.

HPMA-Lac_{m+1} mixture

The monomer was synthesized by stirring L-lactide (4.998 g, 1 equivalence) and HPMA (5.000 g, 1 equivalence) in a round bottom flask in a 130 ℃ oil bath under a N_2 flow for 2 h. $Sn(Oct)_2$ (0.141 g, 0.01 equivalence) and 4-methoxyphenol (0.004 g, 0.001 equivalence) were dissolved in 0.1 mL anhydrous toluene and added to the reaction mixture.[44] The round bottom flask was baked at 130 ℃ overnight and de-gassed under vacuum and nitrogen alternating cycles after loading the reactants. This method generated a mixture of HPMA-Lac_{m+1}, with m = 1, 3, 5. Once the reaction was completed, the product was purified and separated using silica column chromatography and thin layer chromatography (TLC). The separation of the mixture was optimized. The method optimizations were illustrated in Figure S2-S6.

HPMA-Lac$_6$

A modified synthesis yielded a monomer product mainly consisting of HPMA-Lac$_6$. L-lactide (9.996 g, 2 equivalence), HPMA (5.000 g, 1 equivalence), Sn(Oct)$_2$ (0.141 g, 0.01 equivalence) and Na_2SO_4 (0.010 g, 0.002 equivalence) were mixed and heated to 110 ^oC for 16 h under a N_2 atmosphere.[52] After the reaction was completed, the product was purified by participating in cyclohexane. The purified product was dried under a vacuum.

1.2.2.3 Synthesis of macoinitiators (NH_2-PEG)$_2$-ACVA and (PBA-PEG)$_2$-ACVA

The macroinitiators were synthesized by an esterification reaction between NH_2-/PBA-PEG and ACVA. 2 equivalent of NH_2-/PBA-PEG and 1 equivalent of ACVA were dissolved in 5 mL of anhydrous DCM. Meanwhile, 0.3 equivalent of DP and 0.3 equivalent of TS were separately dissolved in 0.1 mL of THF. Then, the mixture was added into NH_2-/PBA-PEG and ACVA solution and purged with N_2 while stirring on an ice bath for 30 min. 3 equivalence of DCC (dissolved in 0.5 mL of anhydrous DCM) was added dropwise to the reaction mixture at 0 ^oC. The reaction was then moved to 25 ^oC and stirred for 16 h. The following day, urea salts were filtered out, and the remaining mixture was vacuum-dried. Finally, the solid product was dissolved in MiliQ water and purified by dialyzing against Mili-Q water.

1.2.2.4 Synthesis of diblock copolymers NH_2-PEG-*b*-(HPMA-Lac$_6$) and PBA-PEG-*b*-(HPMA-Lac$_6$)

The diblock copolymer, polyethylene glycol-*b*-(N-(2-hydroxypropyl) methacrylamide-co-oligolactate) (PEG-*b*-(HPMA-Lac$_6$)), is composed of a hydrophobic N-(2-hydroxypropyl) methacrylamide derivatized with a monodisperse oligolactide (HPMA-Lac$_6$) block and a hydrophilic PEG block. PEG-*b*-(HPMA-Lac$_6$) copolymers were synthesized through a free radical

polymerization,[107] using HPMA-Lac_6 as a monomer and $(NH_2\text{-PEG})_2$-ACVA or $(PBA\text{-PEG})_2$-ACVA as a macroinitiator, respectively. In the polymerization process, the monomer and macroinitiator maintained a molar ratio of 200:1.

1.2.2.5 Formation of drug-loaded and non-drug-loaded MCs

Drug-loaded MCs were prepared by a solvent evaporation method. MCs formed by PBA-copolymer (PBA-MC) and by NH_2-copolymer (NH_2-MC) loaded with LE are denoted as PBA-MC-LE and NH_2-MC-LE. Initially, 10 mg of copolymer with and without PBA end group (dissolved in 970 µL of acetone) and 1 mg of LE (dissolved in 30 µL DMSO) were mixed and incubated at 37 ºC for 30 min. The copolymer-drug mixture was then added dropwise into the ammonium acetate buffer (AAB, 120 mM, pH 5), followed by stirring at 25 ºC for 30 min. Subsequently, the mixture was stirred at 45 ºC for 2 h. To facilitate the evaporation of the solvent, the vial was uncapped and stirred overnight in the hood at 25 ºC. Non-drug-loaded MCs, both PBA-MC and NH_2-MC, were prepared with the same method but without adding the drug.

1.2.3 Characterization

1.2.3.1 ^{1}H NMR spectroscopy

The ^{1}H NMR spectroscopy of tBoc-NH-PEG, NH_2-PEG, PBA-PEG, macroinitiators, monomers, and copolymers was conducted using a Brucker AV 400 MHz NMR Spectrometer (128 scans, 2-second delay). The chemical shift of $CDCl_3$ at 7.26 ppm and $(CD_3)_2SO$ at 2.50 ppm were used to calibrate the reference line. The percent conjugation efficiency of PBA onto NH_2-PEG, the number of average Lac repeating units (m), the number of hydrophobic blocks (x), the average molecular weight of the hydrophobic block (Mw-b), and the average molecular weight of copolymer (Mw-cop) were determined by ^{1}H NMR through the following equations (1-5):

$$\text{Conjugation Efficiency\%} = \frac{I_{\text{benzen-H}}/4}{I_{\text{PEG-H}}/296} \times 100\% \quad (1)$$

$$m = \frac{I_{\text{Lac repeat unis-H}}}{I_{\text{Lac tail-H}}} \quad (2)$$

$$m = \frac{I_{\text{Lac repeat units-H}}}{I_{\text{HPMA vinyl-H}}/2} \quad (2.1)$$

$$x = \frac{I_{\text{Lac tail-H}}/1}{I_{\text{PEG-H}}/296} \quad (3)$$

$$\text{Mw-b} = \%\text{Lac}_6 \times \text{Mw-Lac}_6 + \%\text{Lac}_4 \times \text{Mw-Lac}_4 + \%\text{Lac}_2 \times \text{Mw-Lac}_2 \quad (4)$$

$$\text{MW-cop} = \text{Mw-PEG} + x \times \text{Mw-b} \quad (5)$$

$I_{\text{benzen-H}}$ represents the integration of the total areas of the 4 benzene protons on the PBA. $I_{\text{PEG-H}}$ corresponds to the integrated area of 296 protons on PEG repeating units. $I_{\text{Lac repeat units-H}}$ denotes the integrated area of Lac repeating units —[COCH(CH_3)O]— (at 5.12 – 5.26 ppm), and $I_{\text{Lac tail-H}}$ represents the integrated area of the proton at the tail —COCH(CH_3)OH (at 4.30 ppm) of the HPMA-Lac_{m+1} monomer. Each HPMA-Lac_{m+1} monomer forms a hydrophobic block within the copolymer after free radical polymerization. Molecular weights of different monomers (HPMA-Lac_6, HPMA-Lac_4, HPMA-Lac_2), denoted as Mw-Lac_6, Mw-Lac_4, and Mw-Lac_2, are 575, 431, and 287 g/mol. The percentage of each monomer is calculated from the ^{1}H NMR.

1.2.3.2 Dynamic light scattering (DLS) and zeta potential of MCs

Freshly prepared micellar dispersions were concentrated using a protein concentrator, diluted with PBS (pH 7.4), and filtered with a 0.45 μm filter to prevent dust contamination and MC aggregations. The sizes of the MCs were analyzed with dynamic light scattering (DLS) on a Malvern Zetasizer Nano-Z instrument (Malvern Instruments, Malvern, UK). For each sample,

three measurements were performed under standard operating procedure parameters (25 °C with 20-second equilibration time).

The Zeta potential of the MCs was determined at 25 °C using a Malvern Zetasizer Nano-Z (Malvern Instruments, Malvern, UK) equipped with universal ZEN 1002 'dip' cells and DTS (Nano) software (version 4.20). Zeta potential measurements were performed in PBS at pH 7.4 at a final polymer concentration of 333 µg/mL.

1.2.3.3 Transmission electron microscopy (TEM) of MCs

The TEM images of MCs were taken using T12 Quick room temperature TEM with 120 kV electron-beam energy. The samples are dispersed in Milli-Q water for TEM measurements, then dropped and dried on carbon-coated copper grids.

1.2.3.4 Assessment of drug encapsulation efficiency and loading capacity of MCs

The amount of the loaded anti-inflammatory drug, Loteprednol Etabonate (LE), in the polymeric MCs was determined using High-Performance Liquid Chromatography (HPLC). A standard curve was obtained using LE dissolved in ACN at concentrations ranging from 0.01 to 0.1 mg/mL. The concentrations of LE solutions were measured using HPLC with an ACN/water gradient solvent system at 242 nm. HPLC was run using water without acid as solvent A and acetonitrile without acid as solvent B. Column (5C18-MS-II, 4.6ID x 250mm) was used at 1 mL/min flow rate, with a 70%-90% solvent B gradient for 10 min. The set inject volume into the HPLC was 5µl per sample. A higher concentration than 0.1 mg/mL or a higher injection volume per sample caused the peaks will max out of the measurable range of the instrument.

The freshly prepared MCs were centrifuged at 4000 rpm at 20 °C for 10 min to separate the MCs-LE supernatant and the unencapsulated LE pellet. After the centrifuge process, the supernatant was

carefully pipetted out. The LE pellet was dissolved in 1 mL ACN and diluted 10 fold. The concentration was measured by HPLC using the same method as the measurements of the samples of the standard curve.

The encapsulation efficiency (EE%) and loading capacity (LC%) were calculated using equations (6) and (7), respectively:

$$EE\% = (1 - \frac{\text{unencapsulated drug}}{\text{total drug added}}) \times 100\% \quad (6)$$

$$LC\% = (1 - \frac{\text{unencapsulated drug}}{\text{total copolymer added}}) \times 100\% \quad (7)$$

1.2.3.5 Release study of LE

After separating the MCs from the unencapsulated LE pellet by centrifugation, the supernatant was concentrated to 100 μL using a protein concentrator with a specified molecular weight cutoff (MWCO 100 kDa). Subsequently, it was mixed with 900 μL of an eye drops solution to obtain a 10 mg/mL MCs solution. The eye drops solution was made of hyaluronic acid, glycerin, hypromellose, purified water, benzalkonium chloride, and buffering systems based on the ophthalmic formulations.[53-56] To conduct the release study, 1 mL of MCs solution was pipetted into a dialysis bag (MWCO 12 kDa), and the bag was submerged in 10 mL of artificial tear solution placed in a falcon tube. The falcon tube was then placed in a shaker at 37 °C and gently shaken at 80 rpm for 15 days. To monitor the release of LE into the artificial tear solution, 2 % non-ionic surfactant Triton X-100 was added to the solution to enhance the solubility of LE. At predetermined time intervals (0 h, 2 h, 6 h, 24 h, 2 days, 3 days, 5 days, 7 days, 9 days, 12 days, 15 days), 2 mL artificial tear was sampled, and an equal volume of fresh release media was

replenished. The samples were freeze-dried, re-dissolved in ACN, and their concentration was measured by HPLC using the same method described in 1.1.3.4.

1.2.4 *In vitro* mucoadhesion tests

1.2.4.1 Mucin-targeting evaluation via zeta potential

Commercially available porcine gastric mucin was prepared as a 1 mg/mL solution with Mili-Q water. The solution was then incubated in a 37°C oven for 2 h to ensure complete dissolution. Subsequently, a series of MC solutions with varying concentrations (6, 3, 0.75, 0.18, 0.09 mg/mL) was mixed with 1 mL of mucin solution and 100 mM KCl, then shaken at 37°C for 1 h. After centrifugation and filtration using a 0.2 μm filter, the zeta potential of the mixed solutions was measured.

1.2.4.2 Mucin-targeting evaluation via turbidity

Porcine gastric mucin was prepared as a 1 mg/mL solution with MiliQ water using a probe-type sonicator (FisherBrand) at 500 watts, 20kHz. Sonication was performed at a 5-second interval after every 15 seconds of sonication until the mucin was completely dissolved. PBA-MC and MC are suspended in PBS (1 mg/mL, pH = 7.4). The MC and mucin solutions were mixed to achieve various MCs to mucin ratios (0.1, 1, 2, 3, 10, w/w) and vigorously vortexed for 1 min. The optical density at 600nm (OD 600nm) of PBS and MCs/mucin solutions was measured by a UV-vis spectrophotometer (Thermo Scientific, NanoDrop One^{C}).

1.2.4.3 Mucin-targeting evaluation via spectrofluorometer

First, the suitable excitation wavelength and the emission wavelength range were determined by a spectrofluorometer (Photon Technologies International QuantaMaster) using 0.01 mg/mL PBA-copolymer solution. Then, PBA-bearing MC suspensions were mixed with varying concentrations

(0, 0.02, 0.05, 0.1, 0.2, 0.5 mM) of SA solutions to achieve constant final attention of PBA-MC (50 μg/mL). The mixtures were vortexed for 30 s before measurement with a plate-reader-type spectrofluorometer (Tecan Infinite M1000 Pro). The samples were excited at 295 nm, and an emission scan from 335 to 435 nm was obtained for each sample.

1.2.5 *In vitro* biocompatibility tests

Human corneal epithelial cells (passage 51) were seeded in a 48-well plate. 0.3 mL of alveolar epithelial cell medium (with 2% fetal bovine serum, 1% penicillin/streptomycin, and 1% cervical epithelial cell medium) and 0.03 mL of 300 mg/mL PBA-/NH_2-MC was added to each well. The cells were incubated in a 37 °C oven.

1.2.5.1 Live/Dead assay

In a dark environment, a dye solution was made (0.5 μL/mL calcein and 2 μL/mL ethidium homodimer in PBS). The media in the well of the 48-well plate was carefully pipetted out, and 0.1 mL of the dye solution was added. The 48-well plate was covered with aluminum foil and incubated for 20 min. Then, the dye solution was removed and replaced with 1 mL PBS. The images were taken with a fluorescence optical microscope (Primovert, Zeiss).

1.2.5.2 Actin/DAPI assay

The cells were fixed with Paraformaldehyde 4% and incubated at 25 °C for 20 min, followed by three washes with PBS. Triton X-100 (0.3% w/v, in PBS) was added into each well of the 48-well plate, incubated at 25 °C for 30 min, followed by three washes with PBS. Bovine serum albumin (1%, in PBS) was added and incubated at 25 °C for 1 h. In a dark environment, phalloidin was diluted in 1% bovine serum albumin in a 1 : 400 ratio (2.5 μL/mL actin) and added to each well. The 48-well plate was incubated at 25 °C for 45 min, followed by two washes with PBS. DAPI

was diluted in PBS in a 1 : 1000 ratio (1 μL/mL DAPI) and added to each well. The 48-well plate was incubated at 37 °C for 10 min, followed by two washes with PBS. The images were taken with a fluorescence optical microscope (Primovert, Zeiss).

1.3. Results and discussion

Targeting MC through PBA functionalization was synthesized by multiple steps. First, PBA was conjugated onto PEG with an amine chemical handle. Then, PBA-PEG was reacted with ACVA azo-initiator via a DCC/DMAP coupling reaction, resulting in a macroinitiator $(PBA\text{-}PEG)_2$-ACVA. Separately, a monomer HPMA-Lac_6 was synthesized using a ring-opening method.[44] Finally, the amphiphilic block copolymer (PBA-PEG-b-(HPMA-Lac_6)) was synthesized by a free radical polymerization of HPMA-Lac_6 monomer initiated by $(PBA\text{-}PEG)_2$-ACVA macroinitiator. The resulting copolymer was used to form drug-loaded PBA-MC through a solvent evaporation method. PBA can form covalent interaction with the glycoprotein and sialic acid of the corneal mucin and anchor PBA-MC onto the ocular surface. Therefore, PBA-MC has the potential to improve the retention time of the micellar drug delivery system in the eyes.

1.3.1 Synthesis and characterization

1.3.1.1 Synthesis and characterization of PBA-PEG

PBA-PEG was synthesized by conjugating PBA and amine-PEG with an EDC/NHS catalytic amidation (Figure 2A). Without EDC/NHS activation, the primary anime of NH_2-PEG is not a strong enough nucleotide to directly attack the carboxyl carbon of PBA; the hydroxy group on the carboxyl carbon is also an unstable leaving group, further hinders the direct conjugation.[57] In the presence of EDC, the carboxyl group of PBA becomes the nucleophile, attacks the carbodiimide group (—N=C=N—) of EDC, and forms an intermediate O-acylisourea. Then, NHS reacts with

the carbonyl and replaces O-acylurea with an NHS-ester. The NHS-ester intermediate is crucial for facilitating carboxyl acid and amine conjugation due to its high reactivity. Amine of NH_2-PEG can then react with the NHS-ester. Both products (amide and NHS) exhibit resonance stabilization of electrons among N—C=O structures. Therefore, the reaction favors amide formation.[57] A two-step method is widely used for EDC/NHS activated conjugation between carboxylic acid and a primary amine, as the activation step favors a slightly acidic condition and the amine conjugation step requires a neutral-to-basic pH to occur, as a charged amine does not display good nucleoticity.[58, 59] In some studies, a one-step method is employed to avoid excess waste and successful conjugations were reported using buffer solutions with pH = 6,[60] pH = 7,[61] and pH = 9.[62] The optimal ratio of EDC : NHS is reported at the range of 5:3 to 4:1.[63, 64]

The conjugation efficiency was characterized by ^{1}H NMR spectroscopy in $(CD_3)_2SO$ (Figure 2B) and in $CDCl_3$ (Figure S1). Modifications of parameters and the outcomes were included in Table 2. Initially, due to the low solubility of PBA in aqueous solution, it was dissolved in 0.1 M MES buffer (pH = 4.5) and heated to 90 °C. The temperature was then cooled to 60 °C before adding EDC and NHS. The conjugation efficiency was low (17.5%), as shown by the ^{1}H NMR spectrum (i) in Figure 2B. Previous literature reported that the optimal pH for EDC to react with carboxylic acids is 3.5-4.5,[58, 65, 66] likely due to the stronger nucleophilicity of a deprotonated carboxyl group at a low pH compared to a protonated one. Thus, the activation buffer (0.1M MES) was initially set at pH 4.5. However, the conjugation efficiency was low. Upon closer investigation, it was found in the literature that EDC reacts with carboxyl acid to form an intermediate O-acylisourea, which allows for amine coupling.[67] This O-acylisourea is not only easily rearranged into a N-acylurea, which is not reactive to amine, but also more prone to hydrolysis. Thus, acidic conditions (e.g., pH 3.5-4.5) are favorable for using EDC alone as an activation agent. However, introducing

NHS as a second activation agent converts the O-acylisourea into a NHS-ester, which is not rearrangeable and less prone to hydrolysis. EDC/NHS activation is well developed to suit different amine-barring systems, and the optimal pH often falls into the range of 5-6.[63, 64, 68-71] In another attempt, PBA was dissolved in 0.1 M MES buffer (pH = 6) and heated to 90 °C. The dissolution of PBA decreased the pH of the solution to 5. The temperature was then cooled to 55 °C and EDC was added. After 20 min, NHS was subsequently added. Switching to a less acidic buffer improved the conjugation efficiency to 44.8%, as shown in the ^{1}H NMR spectrum (ii) in Figure 2B.

However, pH is not the only condition that affects the conjugation efficiency. The formation of NHS-ester intermediate is crucial for facilitating carboxyl acid and amine conjugation due to its high reactivity. A high temperature (> 50 °C) favors NHS-ester hydrolysis instead of reaction with amine.[57] To prevent PBA from precipitating after the solution temperature dropped to 45 °C, DMSO was used as a solvent for PBA dissolution. The temperature was set to 45 °C for EDC/NHS activation. The amount of PBA used (25.5 mg) could be easily dissolved in 0.1 mL DMSO. The final concentration of PBA was 0.14 M after mixing with other reagents. In the contract, it requires 2 mL MES buffer to dissolve the same amount of PBA properly, and the final concentration is 0.04 M after mixing with other reagents. The conjugation efficiency was improved to 91.5% after dropping the EDC/NHS activation step temperature, as shown in the ^{1}H NMR spectrum (iii) in Figure 2B. The conjugation efficiency was determined by calculating the integration ratio between benzene protons of PBA (peaks at 7.84 and 7.79 ppm) and protons of the PEG repeating units (between 3.71 - 3.38 ppm) in $(CD_3)_2SO$, using equation (1):

$$\text{Conjugation Efficiency\%} = \frac{\mathrm{I}_{\text{benzen-H}} / 4}{\mathrm{I}_{\text{PEG-H}}/296} \times 100\% = \frac{(1.86+1.80) / 4}{296/296} = 91.5\%$$

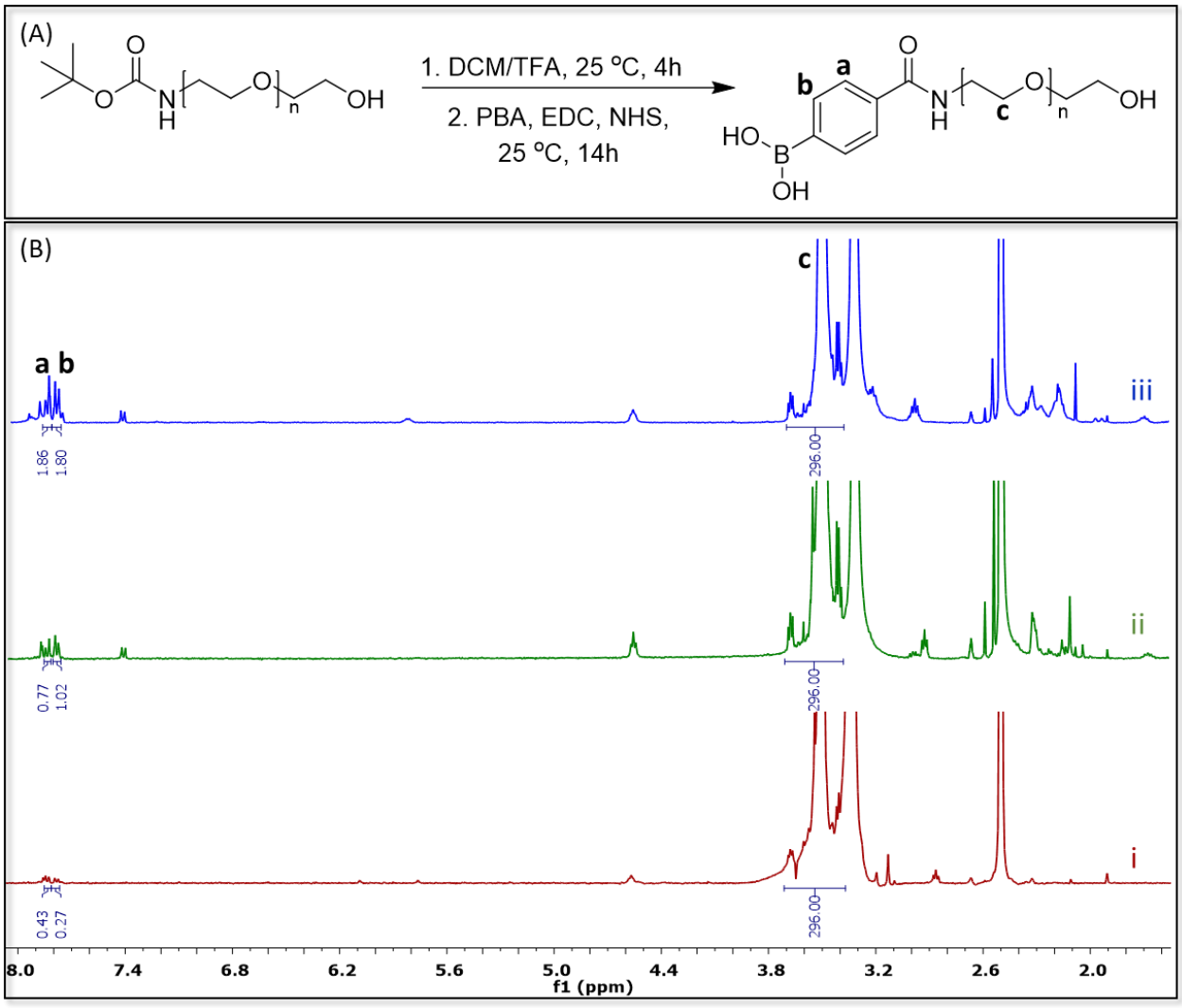

Figure 2. (A) Synthesis of PBA modified PEG; (B) ^{1}H-NMR spectrum of PBA conjugated PEG obtained by different reaction conditions in $(CD_3)_2SO$.

Table 2. Synthesis of PBA-modified PEG in different activation conditions to increase conjugation efficiency of PBA to PEG. During all trials, the activated PBA and amine-PEG conjugation were conducted at pH 7, 25 °C for 14 h.

Trial	Solvent	Activation pH	Activation T (°C)	Efficiency %
i	MES	4.5	60	17.5
ii	MES	6	55	44.8
iii	DMSO/MES	6	45	91.5

1.3.1.2 Synthesis of monomer HPMA-Lac_{m+1}

As previously mentioned, a degradable hydrophobic HPMA-Lac_6 monomer was obtained via a ring-opening polymerization (ROP) between HPMA and L-lactide catalyzed by $Sn(Oct)_2$ as previously reported.[1, 44] This synthesis method yielded a mixture of HPMA-Lac_{m+1}. As the monomers were used to synthesize amphiphilic copolymer, different numbers of Lac repeating units contributed to various hydrophobic chain lengths of the copolymer. In order to verify whether MCs made of copolymers with longer hydrophobic chain lengths can lead to better encapsulation efficiency of non-polar drugs, the first step is to separate the mixtures of monomers.

Silica column chromatography and TLC were used to separate the mixture of monomers. Four modified methods were used, and the results are illustrated in (Figure S2-S5). Method 4 is the optimized method for separating different HPMA-Lac_{m+1} (Figure S5). During the solvent rinsing, method 4 used the slowest solvent gradient change among these four methods. An evident and broad absorbance peak was observed in the 242 nm channel monitor of silica column chromatography, suggesting the products were well-separated. This was because increasing the solvent B% gradually increased the separation of monomers with different degrees of hydrophobicity. The unreacted HPMA, which is more hydrophilic than HPMA-Lac_{m+1}, was flushed out of the silica column last due to the highest high affinity to silica gel. The more Lac repeating units present in a monomer, the more hydrophobic it is, which is expected to be flushed out of the column slower. Due to its hydrophobicity, the unreacted L-lactide was flushed out of the column first. Hydrophobic species ran faster in TLC due to the low affinity of these species to the silica board. HPMA was used as a reference. A series of separated bands were observed on the silica board. Some samples consist of mainly the fast-running bands, some contain bands that run at a medium speed, and some have bands at the slower end. This result confirmed that the monomer

products were well-separated. The separated monomers were characterized by ^{1}H NMR spectroscopy (Figure S6).

Instead of separating the mixture, a modified monomer synthesis was used later. By increasing the ratio of lactide: HPMA from 1:1 to 2:1 and allowing the reaction happened at a lower temperature for longer, a product consisting of mainly HPMA-Lac_6 was obtained and characterized by ^{1}H NMR spectroscopy (Figure S7), which was consistent with HPMA-Lac_6 obtained through silica column separation (Figure S6, spectrum a). NMR results showed the integration ratio between the repeating Lac units protons and the protons at the tail of HPMA- Lac_{m+1} monomer was used to calculate the average Lac repeating units (m), which was found as m = 5 using equation (2):

$$m = \frac{I_{\text{Lac repeat units}-H}}{I_{\text{Lac tail}-H}} = \frac{4.95}{1.05} = 5$$

Alternatively, the integration ratio between the repeating Lac units protons and the vinyl protons at the HPMA part can also be used to calculate average Lac repeating units (m), and it was also found as m= 5 using equation (2.1), which was consistent with the previous calculation.

$$m = \frac{I_{\text{Lac repeat units}-H}}{I_{\text{HPMA vinyl}-H}/2} = \frac{4.95}{(1.00+1.03)/2} = 5$$

1.3.1.3 Synthesis and characterization of $(PBA\text{-}PEG)_2$-ACVA, and PBA-copolymer

PBA-functionalized PEG was conjugated with ACVA azo-initiator via a DCC/DMAP coupling reaction, forming hydrophilic macroinitiator $(PBA\text{-}PEG)_2$-ACVA, as shown in Figure 3A. The characterization of $(PBA\text{-}PEG)_2$-ACVA macroinitiator was performed using ^{1}H NMR spectroscopy in $CDCl_3$, which revealed characteristic signals of PBA at 7.91 and 7.81 ppm, protons

adjacent to ester oxygen at 4.26 ppm, and protons within PEG repeating units —[CH_2CH_2O]— between 3.44 – 3.84 ppm (Figure 3B).

Finally, the amphiphilic block copolymer (PBA-PEG-*b*-(HPMA-Lac_6)) was synthesized by a free radical polymerization of HPMA-Lac_6 monomer initiated by $(PBA\text{-}PEG)_2$-ACVA macroinitiator (Figure 3A). The polymerization was carried out in anhydrous acetonitrile (ACN) at 70 °C for 24 h. The successful synthesis of PBA-PEG-*b*-(HPMA-Lac_6) block copolymers was confirmed by ^1H NMR analysis in $CDCl_3$. Characteristic peaks corresponding to the PEG repeating units appeared between 3.44 and 3.84 ppm, while peaks attributed to the Lac repeating units of HPMA-Lac were observed between 5.12 and 5.26 ppm. Moreover, PBA groups located at the end of the copolymer chain were clearly identified at 7.92 and 7.81 ppm (Figure 3C).

The number of hydrophobic blocks (x) in the copolymer was determined by the integration ratio between the protons at the tail of the HPMA-Lac_6 monomer and protons in the PEG repeating units, resulting in 37. The average molecular weight of the hydrophobic block (Mw-b) was calculated (518.7 g/mol). Additionally, the average molecular weight of the copolymer (Mw-cop) was calculated as 22591.9 g/mol. These results were obtained through the equations (3-5) shown below:

$$x = \frac{I_{\text{Lac tail}-H} / 1}{I_{PEG-H}/296} = \frac{0.24 / 1}{1.92/296} = 37$$

$$\text{MW-b} = \%Lac_6 \times \text{MW-}Lac_6 + \%Lac_4 \times \text{MW-}Lac_4 + \%Lac_2 \times \text{MW-}Lac_2$$

$$= 75.2\% \times 575 + 10.5\% \times 431 + 14.3\% \times 287 = 518.7$$

$$\text{MW-cop} = \text{MW-PEG} + x \times \text{MW-b} = 3400 + 37 \times 518.7 = 22591.9$$

As a control group, we also synthesized a block copolymer using HPMA-Lac_6 monomer and $(NH_2\text{-}PEG)_2$-ACVA macroinitiator devoid of PBA groups based on the procedure explained previously.

Initially, $(NH_2\text{-}PEG)_2$-ACVA macroinitiator was synthesized and the ^{1}H-NMR spectrum is given in Figure S8. Thereafter, similar to PBA-bearing copolymers, the polymerization was carried out in anhydrous ACN for 24 h at 70 °C. The obtained copolymer (NH_2-PEG-*b*-(HPMA-Lac_6)) was characterized by ^{1}H-NMR spectroscopy Figure S9.

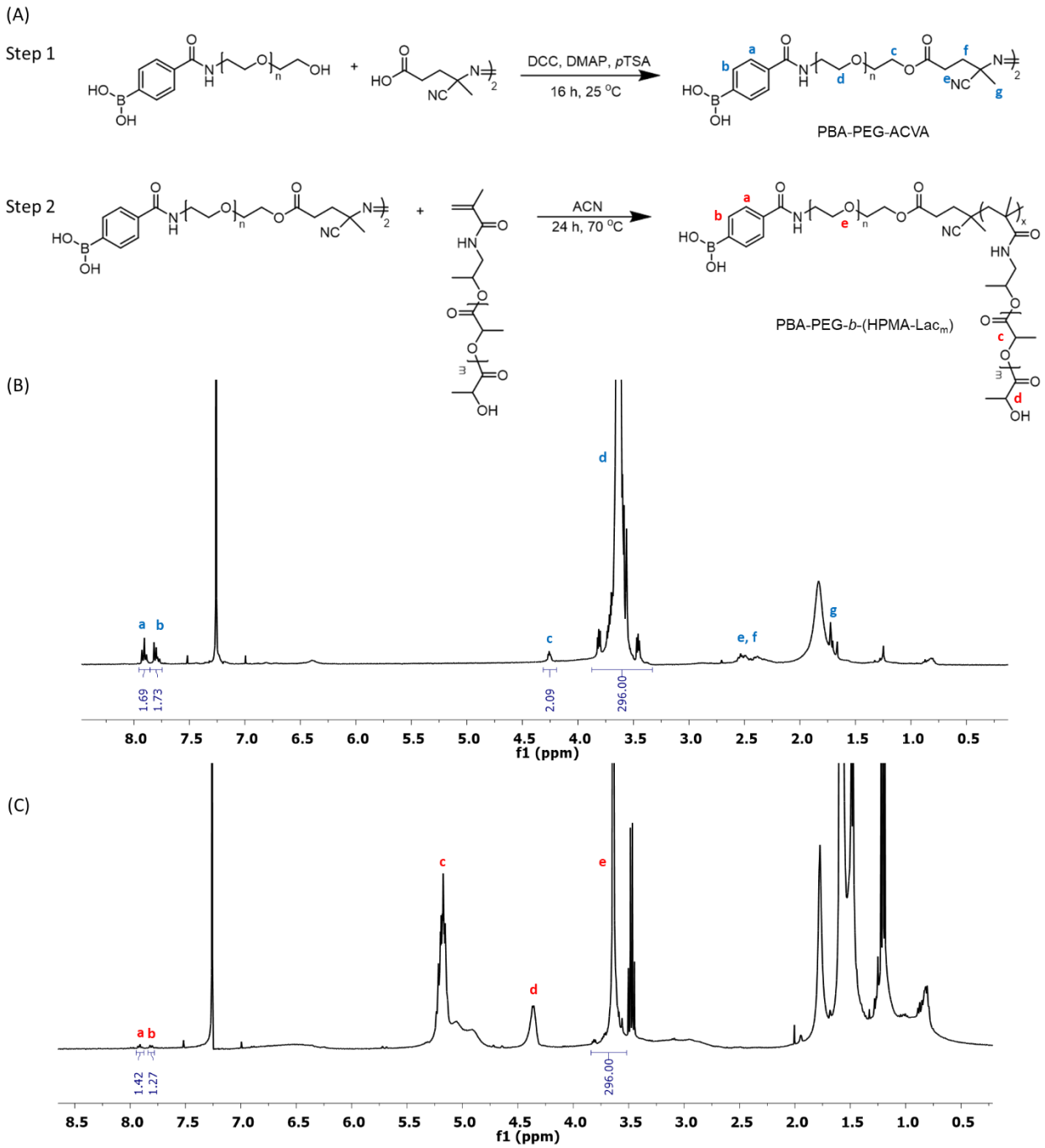

Figure 3. (A) Synthesis of PBA-PEG-ACVA macroinitiator via DCC/DMAP coupling and block copolymer PBA-PEG-*b*-(HPMA-Lac$_6$) via free radical polymerization; (B) ^{1}H-NMR characterization of PBA-PEG-ACVA macroinitiator; and (C) ^{1}H-NMR characterization of PBA-PEG-*b*-(HPMA-Lac$_6$) copolymer in $CDCl_3$.

1.3.1.4 Synthesis and characterization of MCs

The copolymers, with and without PBA end groups, were used to self-assemble into micellar structures using a solvent evaporation method (Figure 1A). The copolymers were dissolved in acetone and then dropped into AAB. The self-assembly of MCs was induced through an entropy-driven phenomenon. The amphiphilic copolymers were exposed to an aqueous environment as the organic solvent evaporated. The hydrophobic blocks of the copolymers exhibited an unfavorable interaction with water molecules, resulting in the formation of a rigid water cage around the hydrophobic blocks, leading to low entropy. As the hydrophobic blocks started to entangle with each other, less surface area was exposed to water. Consequently, some water molecules were released from the rigid cage, leading to increased entropy. The entropy gain drove an increasing amount of hydrophilic blocks to aggregate, eventually forming a hydrophobic core to minimize interactions with water. Meanwhile, the hydrophilic PEG blocks remained at the outer layer, forming the hydrophilic shell of the MCs. The hydrophobic core of the MCs, composed of HPMA-Lac_6, enabled the encapsulation of various hydrophobic drugs such as doxorubicin, paclitaxel, etc.[72] In this study, we encapsulated an anti-inflammatory drug, LE, within the hydrophobic core of MCs formed by PBA-PEG-b-(HPMA-Lac_6) and PEG-b-(HPMA-Lac_6) copolymers. Drug-loaded MCs formulations were obtained by an additional drug dissolution step in which LE was dissolved in DMSO before incubation with copolymers solution.

Hydrodynamic size, PDI, zeta potential, and TEM of MCs

The hydrodynamic sizes of drug-loaded and unloaded MCs were measured using dynamic light scattering (DLS). The hydrodynamic sizes PBA-MC and PBA-MC-LE were measured to be 130.6 ± 0.3 nm with a PDI of 0.064 and 133.8 ± 0.8 nm with a PDI of 0.040, respectively. Similarly, the hydrodynamic sizes of MCs formed by PEG-*b*-(HPMA-Lac_6) copolymers (as a control group)

were also measured. The sizes of unloaded MCs (MC) and LE-loaded micelles (MC-LE) were measured to be 127.4 ± 0.5 nm with a PDI of 0.021 and 127.8 ± 8.1 nm with a PDI of 0.049, respectively (Figure 4A, B No significant difference was observed in size between unloaded and LE-loaded MCs in both PBA and control groups. The size of these MCs was slightly larger compared to published studies using PEG and HPMA-Lac type of copolymer (117.30 ± 0.30 nm by Chen *et al.*[1]). Such a difference is likely resulted from one or both of the reasons: 1. a longer hydrophobic chain length (HPMA-Lac_6) was used in this study compared to HPMA-Lac_n (n = 1, 2, 3) in Chen *et al*.'s study; 2. a 200:1 monomer to macroinitiator ratio was used in this study compared to 150:1 in Chen *et al*.'s study. Macroinitiator is mainly hydrophilic due to the PEG block. Another study by Riley *et al*., reported by a higher polylactide : PEG ratio resulted in significantly larger nanoparticles.[73] Another study by Soga *et al.* examined that by increasing the HPMA-Lac block from 3000 to 13 600 g/mol, the size of the MC decreased first and then increased again.[41] The initial decrease in size could result from a more densely packed hydrophobic core since more hydrophobic interaction can be formed in the presence of more non-polar segments. The increased size could result from too large of a hydrophobic block, eventually overpowering the dense interaction and occupying more space. The low PDIs in this study indicated a high level of homogeneity in the size of the MCs. Typically, the PDIs are below 0.2 (0.17 by Soga *et al*. and 0.094 by Chen *et al*.). Finally, the surface charge of the MCs was determined using a Zetasizer. The zeta potentials of MCs were found as 0.64 ± 0.61 mV, 0.49 ± 0.29 mV, 1.35 ± 0.97 mV, 2.47 ± 0.43 mV for PBA-MC, PBA-MC-LE, NH_2-MC, and NH_2-MC -LE, respectively (Figure 4C). Also, the morphology of drug-loaded PBA-bearing MCs (PBA-MC-LE) and MCs devoid of PBA group (NH_2-MC -LE) was evaluated by TEM (Figure 4E). The average sizes of dried micellar structures were 20 nm, as observed from TEM for PBA-MC and NH2-MC. This was attributed to

the hydrophilic PEG shell, which can retain a large amount of water in the solution. However, the water portion was depleted during the drying process, leading to the observed size reduction in the dried micellar structures.

Drug encapsulation efficiency, loading capacity, and in vitro release from MCs

The amount of LE loaded inside the hydrophobic core of MCs can be regulated by adjusting polymer/LE. A previous study in our group showed that EE% of LE increased as the copolymer/LE ratio decreased. However, no significant differences were observed among groups with a copolymer/LE ratio lower than 10:1 (w/w).[1] Based on these findings, a copolymer-to-LE ratio of 10:1 (w/w) was selected to calculate EE% and conduct *in vitro* release experiments in this work. The EE% and LC% of the drug were determined by HPLC, using a standard curve of LE established at five different concentrations (Figure S10). MC_{lacm+1} represents MC formed by copolymer PEG-*b*-(HPMA-Lac_{m+1}), which was synthesized using a mixture of monomers (HPMA-Lac_{m+1}, m=1,3,5). MC_{lac6} represents MC formed by copolymer PEG-*b*-(HPMA-Lac_6), which was synthesized using monomer HPMA-Lac_6 separated from a mixture.

LE-loaded MC_{lacm+1} and MC_{lac6} were synthesized, and the concentrations of unencapsulated LE were measured using HPLC. The standard curve and measurement of LE absorption peak areas are shown in Figure S5. The calculations of EE% using equation (6) are shown below:

$$EE\%\_MC_{lacm+1} = \left(1 - \frac{\text{unencapsulated drug}}{\text{total drug added}}\right) \times 100\% = (1 - 0.0772 \times 10/1) \times 100\% = 22.8\%$$

$$EE\%\_MC_{lac6} = \left(1 - \frac{\text{unencapsulated drug}}{\text{total drug added}}\right) \times 100\% = (1 - 0.0535 \times 10/1) \times 100\% = 46.4\%$$

MC made from copolymer with a mixture of HPMA-Lac_{m+1} showed an EE% of 22.8%, consistent with a study that used the same MC for anti-inflammatory therapeutic ($25.5 \pm 2.8\%$).[1] As expected,

MC made from copolymer with longer hydrophobic chains (MC_{lac6}) exhibited better EE% of LE (46.4%) compared to MC_{lacm+1}.

After the modified monomer synthesis was implemented, the assessment of EE% was repeated. EE%_MC_{lac6}' denotes the MC formed by HPMA-Lac_6 that was synthesized by the modified synthesis. EE%_MC_{lac6}' of LE was found as 45.8 ± 2.0% for PBA-MC-LE and 46.5% ± 3.2% for MC-LE. Furthermore, the LC% of MCs was calculated as 4.6% ± 0.2% for PBA-MC-LE and 4.7% ± 0.3% for MCs-LE (Figure 4D). EE%_MC_{lac6}' was consistent with EE%_MC_{lac6}—both were more than twice the EE%_MC_{lacm+1}.

As the number of Lac repeating units increased, copolymer PEG-*b*-(HPMA-Lac_6) aggregated with a higher amount of LE in an aqueous environment as the MC_{lac6} formed. This was attributed to the hydrophobic effect and the non-polar nature of LE. Such a phenomenon provides a powerful tool to tune the drug payload for polymeric micelle drug delivery platforms. Further experiments are needed to examine whether this trend can be observed with other non-polar therapeutics, such as prednisolone acetate (PA), dexamethasone (DEX), paclitaxel, and coumarin.

In vitro drug release behavior of PBA-MC-LE and MC-LE in an eye drops solution was studied via a dialysis method using artificial tear[74] as the release medium. The eye drops solution was made of hyaluronic acid, glycerin, hypromellose, purified water, benzalkonium chloride (as a preservative), and buffering systems based on the ophthalmic formulations.[53-56] Hyaluronic acid can provide desirable viscosity, shear thinning behavior, and lubrication; glycerin helps to reduce surface tension; hypromellose provides mucoadhesion, which can extend the retention time of the eye drops on the cornea and allow the targeting moieties to form interaction with the corneal mucin.[53] The MCs were dispersed in 1 mL of eye drops solution and dialyzed against 10 mL of

artificial tear fluid. During the period of release study, 2 mL of artificial tear solution was sampled at each time point, and an equal volume of fresh artificial tear solution (2 mL) was added to maintain a constant total volume. The concentration of released LE in these samples was determined by HPLC. Similar to many drug delivery nanocarriers, PBA-MC showed a two-phase release profile—an initial burst release phase (35.79 ± 4.15% at 12 h, 51.85 ± 3.88% at 24 h) and a slow, non-linear release of up to 100% drugs for 12 days. NH_2-MC released 32.58 ± 3.22%, 47.08 ± 3.89%, and 95.85 ± 4.43% by 12 h, 24 h, and day 12, respectively. Modifying the surface of MCs with PBA did not affect the release profile, as shown in Figure 4F. The MCs completely released their drug payload after 12 days due to the hydrolysis of lactate chains of copolymers. Initial burst release is a common phenomenon for nano-drug carriers. A study utilizing PBA-chitosan oligosaccharide-vitamin E MC showed 75% of the encapsulated coumarin-6 was released at 0.5h, and almost all drugs release at 2 h.[15] In another study, Liu *et al.* used PBA-poly(Lac)-dextran NP and reported near 40% of encapsulated cyclosporine A was released at 12h and about 53% at day 1.[4] In a study that used the PEG-b-(HPMA-Lac_n) MC, the release of LE was 24.2% at 2 h and 53.1% at 24 h.[1] PBA-MC in this work showed a lower release during the first day compared to these studies (especially during the first couple of hours), potentially due to a denser hydrophobic interaction in the core of the MC because the longer Lac chains. However, a study that used poly(lac)-b-poly(methacrylic acid-co-PBA) reported only 35 to 45% encapsulated cyclosporine A released on day 1. Their material incorporated PBA into the repeating units. As MC was formed, the drug and PBA were evenly distributed and it helped to stabilize the drug in the MC.[3] Their result showed that there is room to reduce the initial burst release in our design.

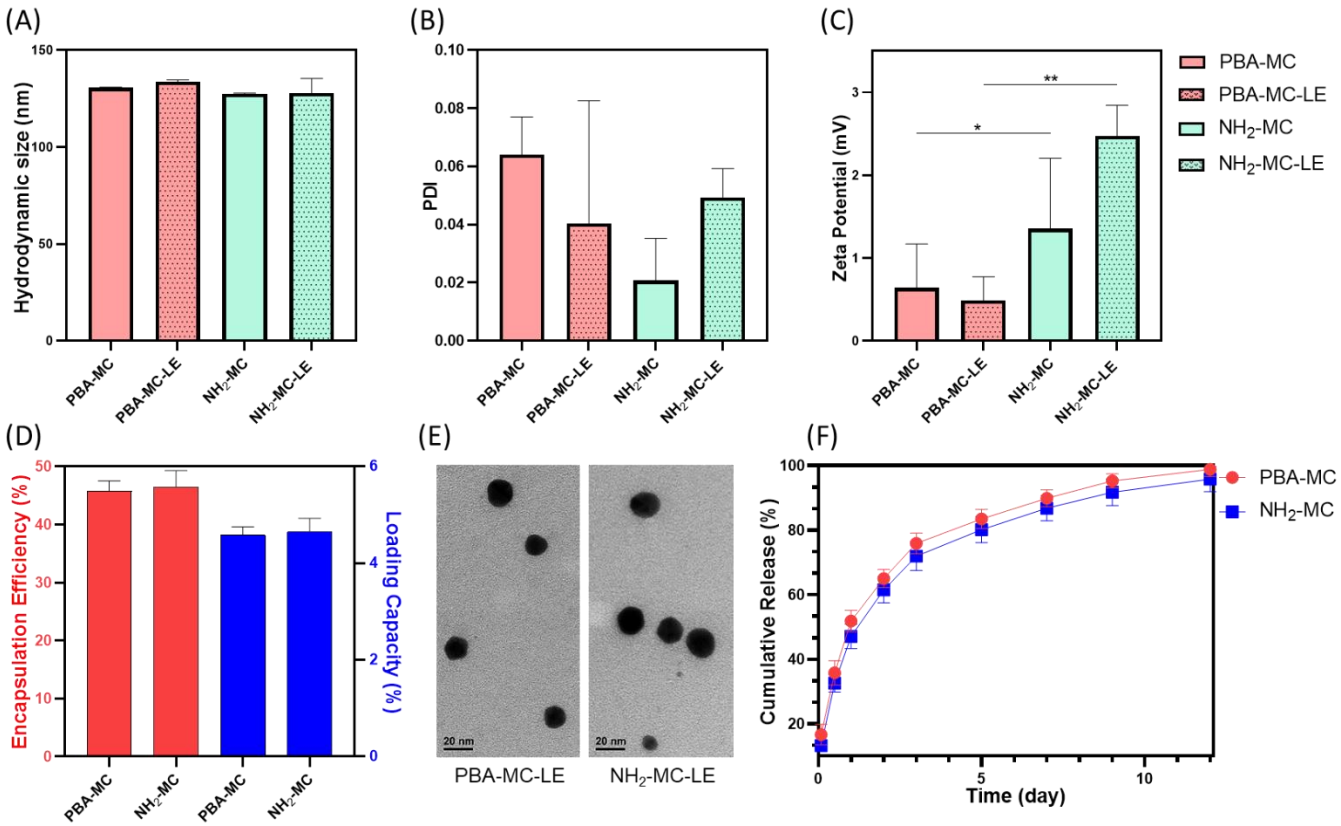

Figure 4. (A) Hydrodynamic size measurements of LE loaded and unloaded MCs; (B) PDI of MCs obtained by Zetasizer; (C) surface zeta potential measurements of MCs; p value < 0.05 (*), p < 0.01 (**); (D) encapsulation efficiency and drug loading capacity of MCs with copolymer/LE ratio 10:1 w/w%; (E) TEM images of PBA-MC-LE and NH_2-MC-LE; (F) *in vitro* release studies of LE from PBA-MC-LE and NH_2-MC-LE at 37 ºC in an artificial tear solution containing 2% Triton X-100.

1.3.2 *In vitro* mucoadhesion studies of PBA-MCs

1.3.2.1 Mucin-targeting effect access via zeta potential

Zeta potential of nanoparticles in the incubation system was employed to predict the mucin binding capacity of the formulations, thereby assessing the mucoadhesive performance.[75] Initially, the zeta potentials of PBA-MC and NH_2-MC were 0.64 ± 0.61, and 1.44 ± 0.88 mV, respectively. Mucin solution (1 mg/mL) without any MCs was measured as -7.01 ± 0.65 mV due to its aspartate and glutamate residues. When MCs were absorbed into the mucin, a decrease in zeta potential would occur due to the negative charge of mucin. A higher zeta potential difference compared to pure MCs solution represents better adhesion. As shown in Figure 5A, the zeta potential of PBA-MC and mucin mixture increased significantly from -7.01 ± 0.65 mV to 3.25 ± 0.63 when increasing the PBA-MCs concentrations from 0 to 0.08 mg/mL. As expected, the zeta potential of NH_2-MC at the same concentration range (0-0.08 mg/mL) did not change by mixing with mucin since there was not a strong interaction between mucin and NH_2-MC due to the lack of PBA group. However, at higher concentrations (>0.3mg/mL), NH_2-MC started to exhibit mucoadhesion properties, although it was significantly weaker than the PBA-MC groups. This is likely due to the amine group on the end of PEG chains. The pKa of the amine-PEG ranges from 9 to 11.[76] Amine end group bears a positive charge at pH below 9, which means it can interact with mucin (bears negative charges due to carboxyl groups and sulfate groups[75, 77]) through ionic interaction.

1.3.2.2 Mucin-targeting effect access via turbidity

Free mucin is a large soluble macromolecule.[78] As MCs with mucoadhesive property form interaction with mucin molecules, they tend to tangle up and aggregate into larger, irregular-shaped granules, which can scatter visible light and reduce the transparency of the solution.[79] The turbidity of mucin solutions was measured after mixing with MCs using UV-vis spectroscopy at OD_{600nm} (Figure 5B). At a 1:10 MCs to mucin ratio (w/w), PBA-MC, NH_2-MC, and PBS (no MCs) groups showed no significant differences. Mucin samples mixed with PBA-MC and NH_2-MC at and above 1:1 MCs/mucin ratios (1, 2, 3, 10) exhibited increased turbidity as the weight ratio of MCs increased. This trend suggests that both PBA groups on PBA-MC and the amine group on NH_2-MC exhibit mucoadhesion properties. At MCs/mucin ratios 1, 2, and 3, PBA-MC induced significantly higher (nearly two folds) changes in the turbidity compared to NH_2-MC, indicating a much better mucoadhesion effect. At a MCs/mucin ratio of 10, PBA-MC led to a further increase of turbidity compared to samples at a MCs/mucin ratio of 3, but with a slower increasing rate. This suggests that the majority of the mucin in the solution formed interactions with PBA-MCs and there was not enough free mucin to support the increasing trend. MC group did not show a significant increase in turbidity at the MCs/mucin ratio of 10 compared to 3, indicating a limited mucoadhesion effect by amine groups alone.

1.3.2.3 Mucin-targeting effect access via spectrofluorimeter

Furthermore, we also investigated the mucoadhesive properties of PBA-modified MC with sialic acid by a fluorescent spectrometer. Sialic acid, abundant in corneal mucin, was chosen because PBA can covalently bind to its cis-diol structure.[80] PBA exhibits an intrinsic fluorescence property. However, its fluorescence will be quenched when PBA forms covalent bonds with a diol group. Such a phenomenon can be monitored via a fluorescent spectrometer to access the binding of PBA

and other diol species.[81-83] PBA can be excited at 295-302 nm and give an emission range between 310-450 nm.[82, 84] The excitation and emission range of PBA-copolymer (0.01mg/mL) was measured by a spectrofluorometer. The excitation and emission can be slightly shifted after the conjugation of PBA to a copolymer. In our case, the peaks of excitation and emission curves were found at 307nm and 354nm, respectively (Figure S6). The emission of PBA-MC (50 μg/mL) before and after mixing with various sialic acid solutions (0, 0.02, 0.05, 0.1, 0.2, 0.5 mM) was measured by a fluorescent plate reader. The fluorescent plate reader was set to measure an emission range between 335-374 nm based on the emission peak (354 nm) found by the spectrofluorometer. The excitation wavelength was set at 295 nm because of the limitation of the instrument. Due to the wide bandwidth of the light bulb in this fluorescent plate reader, the excitation wavelength needs to be set to at least 40 nm, different from the emission scanning range, so that the emission scanning channel does not pick up any excitation signal. It was observed when PBA-MCs were mixed with an increased amount of sialic acids, the fluorescence emission intensity of the solution gradually decreased, as shown in Figure 5C. This result showed that PBA-bearing MC has the ability to bind efficiently to sialic acids in the mucin.

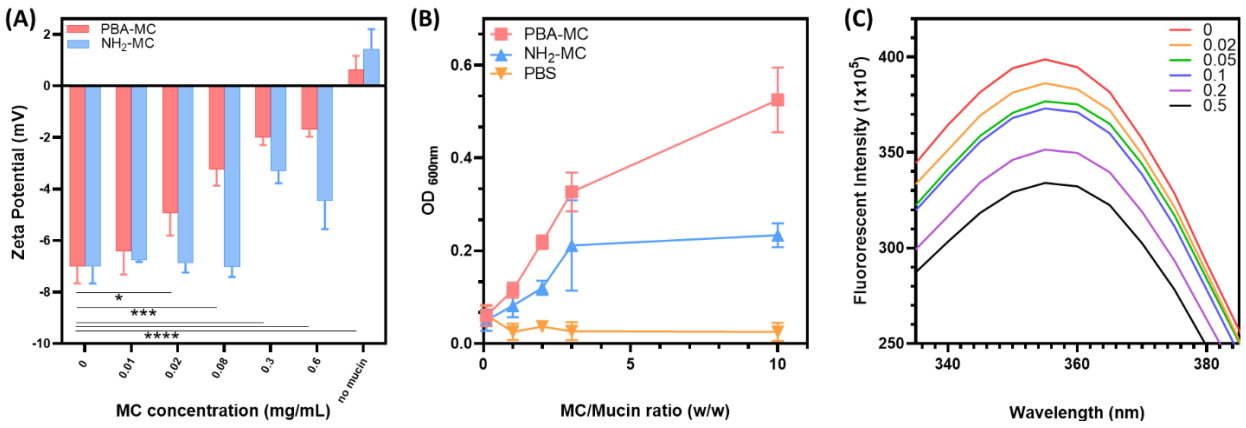

Figure 5. *In vitro* mucoadhesion studies of MCs. (A) zeta potential of mucin solutions before and after the addition of MCs; p value < 0.05 (*), <0.005 (***), and <0.0001 (****); (B) turbidity of mucin solutions measured with various MCs to mucin ratios (0.1, 1, 2, 3, 10, w/w); and (C) fluorescence spectrometer measurement of 50 µg/mL PBA-MCs dispersion mixed with different amount of sialic acid solutions (0, 0.02, 0.05, 0.1, 0.2, 0.5 mM).

1.3.3 *In vitro* biocompatibility studies of PBA-MCs

To assess the biocompatibility of PBA-MC, the viability and metabolic activity of human corneal epithelial cells were examined using Live/Dead and Actin/DAPI assays on day 1 and 5. The cells were exposed to a high concentration of PBA-MC (30 mg/mL), cells without treatment served as a control. The Live/Dead assay results revealed a notable increase in cell numbers and high cell viability (>95%). No significant difference was observed between the PBA and control groups (Figure 6A & B). Additionally, fluorescent staining of the cultured cells demonstrated the spreading and proliferation of cells on the culturing dish, as evidenced by the assembly of actin filaments in the cytoskeleton. These findings indicate the in vitro biocompatibility of the MCs (Figure 6C).

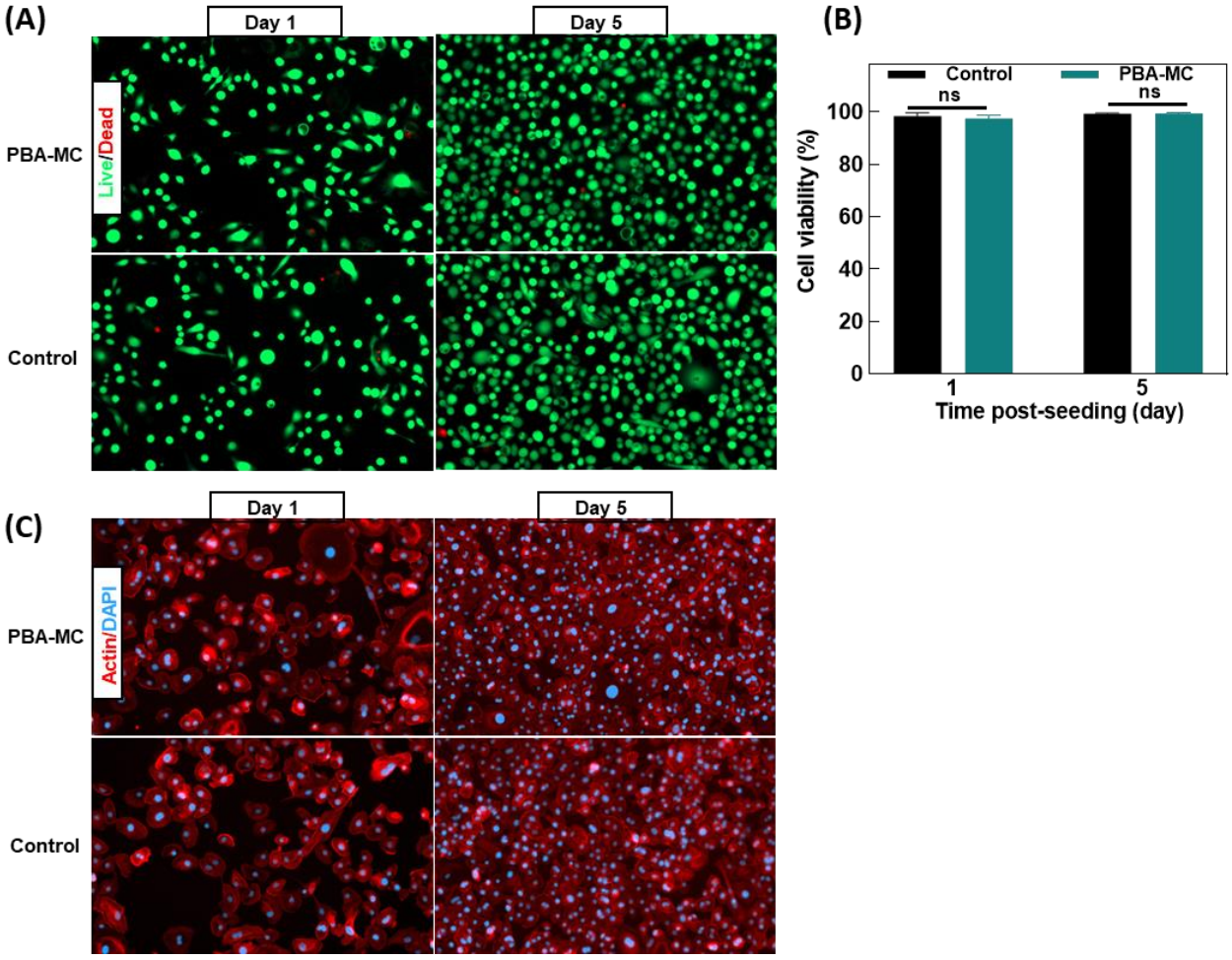

Figure 6. *In vitro* biocompatibility studies of MCs. (A) Representative Live/Dead images from Human corneal epithelial cells cultured with 30 mg/mL PBA-MC and NH_2-MC (control) on day 1 and 5; (B) cell viability% of Human corneal epithelial cells cultured with 30 mg/mL PBA-MC and NH2-MC (control) on day 1 and 5; and (C) Representative Actin/DAPI images from Human corneal epithelial cells cultured with 30 mg/mL PBA-MC and NH2-MC (control) on day 1 and 5.

1.4 Conclusion

In this chapter, a polymeric micellar drug delivery platform was modified and functionalized with an ocular-targeting moiety, PBA, to deliver an anti-inflammatory therapeutic (LE). The MCs were

formed by amphiphilic copolymers, NH_2-PEG-b-(HPMA-Lac_6) and PBA-PEG-b-(HPMA-Lac_6). The amine handle of NH_2-PEG also equipped the NH_2-MC with further potential to conjugate with countless functional groups and cargos. Amine is a volatile functional group that can introduce moieties containing thiol, ketone, epoxide, ether, acetic anhydride, etc. PBA was then conjugated on PEG through the anime chemical handle. The highest conjugation efficiency (91.5%) was achieved by varying the pH, temperature, and solvents of EDC/NHS activation. Using a cosolvent system of DMSO and MES buffer to dissolve PBA allowed for a higher reactant concentration and lower reaction temperature.

PBA functional group can adhere to the cornea by forming covalent bonds with the cis-diol structures on glycoproteins and sialic acids on the corneal mucin. The mucoadhesion ability of PBA-MC was proven by the altered zeta potential and increased turbidity after mixing with mucin. Furthermore, the results of spectrofluoroscopy showed that as PBA on the surface of MC forms covalent bonds with sialic acid, the intrinsic fluorescent of PBA is quenched. The amount of fluorescent signal quenched was positively related to the amount of sialic acid added, suggesting the PBA group present on MC formed covalent bonds with sialic acid. Therefore, PBA-MC demonstrated a promising ability to adhere to sialic acid-abundant mucin. Future experiments should focus on *ex vivo and in vivo* assessments of the mucoadhesion of PBA-MC.

A previous study demonstrated good biocompatibility and an efficient delivery effect for anti-inflammatory drugs using this type of MC. The MC in their study was made of PEG-*b*-(HPMA-Lac_{m+1}) copolymer and the MC was loaded into an adhesive GelPatch before being applied to the eyes.[1] Funtionalizing MC with ocular-targeting moieties allows the MC to adhere to the cornea without the help of the additional patch. Therefore, the targeted micellar drug delivery platform

can be formulated into an eye drops. The eye drops is easier to apply to the eye than a gel patch, which can effectively lower the technical barrier for the patients. Additionally, since the PBA-MC can covalently attach to the corneal mucin, it showed a great potential to stay on the cornea and release encapsulated drugs sustainably over for 12 days as it slowly degrades. Furthermore, the anti-inflammatory drug-loading efficiency was improved. Lastly, Live/Dead assay and Actin/DAPI assay results demonstrated good biocompatibility of PBA-MC. Although future *ex vivo* and *in vivo* experiments are needed, the PBA-MC drug delivery platform is a promising candidate for treating ocular diseases and injuries.

Chapter II. Targeted MCs through GA-functionalization

2.1 Introduction

GA is a phenolic acid with three adjacent hydroxyl groups and a carboxyl group on a benzene ring. It is a natural compound that is produced by a wide range of plants and fungi, such as oak, mango, and papaya, and can be found in animal products like honey.[85, 86] GA exhibits excellent antioxidant, anticarcinogenic, and antimicrobial properties similar to TA. This polyphenol contains multiple GA moieties.[147, 87, 88] Recently, dopamine, tannic acids, and their derivatives have gained lots of spotlight through their outstanding performance on bioadhesive materials; the catechol groups and benzenetriol groups on these compounds can mimic the phenol-rich proteins on mussels, which help them to anchor on the wet and salty surfaces against ocean waves.[89-91] Based on the shared chemical structures (catechol groups and benzenetriol groups), GA is expected to display a similar bioadhesive property as TA and dopamine. Ramirez-Barron *et al.* reported a bioadhesive nanocomposite made of GA-functionalized gelatin for wound dressing.[90] In addition, GA consists of the same carboxyl group as PBA, which was used to conjugate PBA to the MC. Therefore, in this chapter, GA was explored as an alternative to PBA to add bioadhesive properties on MC.

2.2 Materials and methods

2.2.1 Materials

GA and triethylamine (TEA) were purchased from Sigma-Aldrich. The rest of the materials were the same as in section 1.2.1.

2.2.2 Methods

2.2.2.1 Synthesis of GA-PEG

tBoc-NH-PEG-OH was deprotected using the method mentioned in section 1.1.2. After deprotection, NH_2-PEG was purified with diethyl ether washes. At trial vi, GA (8.5 mg), DDC (46 mg), NHS (26 mg), and NH_2-PEG (15 mg) were reacted in THF (3.5 mL). 10 µL TEA was added as a base. The mixture was purged by N_2 and reacted for 14 h. Previous attempts (trial i-v) were made using different concentrations of reactants, solvents, activation reagents, and reaction conditions (Table 3). The product was purified by a vacuum filter, dialyzing against Mili-Q water for 3 days, and obtained by freeze-drying.

2.2.3 Characterization of GA-PEG

The ^{1}H NMR spectroscopy of GA-PEG was conducted using a Brucker AV 400 MHz NMR Spectrometer (128 scans, 2-second delay). The chemical peak of solvent $(CD_3)_2SO$ at 2.50 ppm was used to calibrate the reference line. The percent conjugation efficiency of GA onto NH_2-PEG was determined by ^{1}H NMR through the equations (6) using the same method as chapter I.

$I_{benzen\text{-}H}$ represents the integration of the total areas of the 2 benzene protons on the GA. $I_{PEG\text{-}H}$ corresponds to the integrated area of 296 protons on PEG repeating units.

2.3 Results and discussion

2.3.1 Synthesis and characterization of GA-PEG

GA-PEG was synthesized using GA and NH_2-PEG (Figure 7). During trials i-vi, multiple attempts were made using different reaction conditions (Table 1). At the ^{1}H-NMR spectrum of trials ii-vi, the peak of the two characteristics of benzene protons of GA can be found at 6.91 ppm,[92] suggesting successful conjugation (Figure 7). The three phenyl protons were not visible on the

spectra, which might be because they are labile protons and exchanged with the D_2O in $(CD_3)_2SO$. At trial i, the activation and conjugation steps were conducted in MES buffer (pH 6). At trial ii, the activation step was conducted in DMSO and the conjugation step was conducted in MES buffer (pH 6). Literature reported that pH 5-6 is optimal for the activation step, as the carboxyl group of GA is deprotonated and becomes nucleophilic, while the N on the carbodiimide group (—N=C=N—) of EDC or DCC is protonated, making the C a strong electrophile.[43-46] Meanwhile, for the conjugation step, the amine group on PEG exhibits better reactivity toward the activated carboxyl group at a more basic pH.[58, 59] To simplify the synthesis process, multiple studies explored one-pot method using buffer solutions with pH = 6,[60] pH = 7,[61] and pH = 9.[62] Since gallic acid is unstable at a basic pH,[93] MES buffer (pH 6) was used in trials i and ii. However, trials i and ii yield the lowest conjugation efficiency (0% and 3%), indicating an aqueous environment at pH 6 might not favor the conjugation between GA and amine-PEG. This is likely because, at pH 6, the majority of primary amine is protonated and unable to attack the intermediate. Therefore, at trial iii, both activation and conjugation were conducted in DMSO. DMSO is a polar aprotic solvent, which means it cannot protonate the amine group and is unlikely to oxidize GA to a quinone. The conjugation efficiency of trial iii is increased to 5.5%.

Further optimizations were made using various solvents. DMF is an excellent polar aprotic solvent; it can stabilize polar species via hydrogen bonds, serve as a catalyst, and facilitates SN_2 nucleophilic substitution.[94] EDC/NHS and DCC/NHS catalytic coupling involved multiple SN_2 substitution reactions as the intermediates were formed. Thus, DMF might contribute to the improved conjugation efficiency (41%) in trial iv compared to trial iii. However, a large amount of impurities around 4.2 and 7.7 ppm were observed in trial iv, potentially because DMF is not an

inert solvent, but an active reagent itself and can generate a myriad of functional groups.[94] This result indicated that DMF might not be the optimal solvent.

DCC was used as an alternative to EDC. THF was used by multiple studies as a solvent of DCC/NHS coupling.[95-97] The first attempt (trial v) using DCC yield a low conjugation rate (3.5%). Another attempt (trial vi) added TEA as a base. Since the pH cannot be adjusted in an organic aprotic solvent, a base such as TEA or diisopropylethylamine (Hünig's base) is often used to facilitate a reaction that requires deprotonation.[98-100] In trial vi, the conjugation efficiency was drastically improved compared to trial v (66%), likely because the presence of TEA can deprotonate the primary amine of NH_2-PEG, allowing it to attack the activated GA.

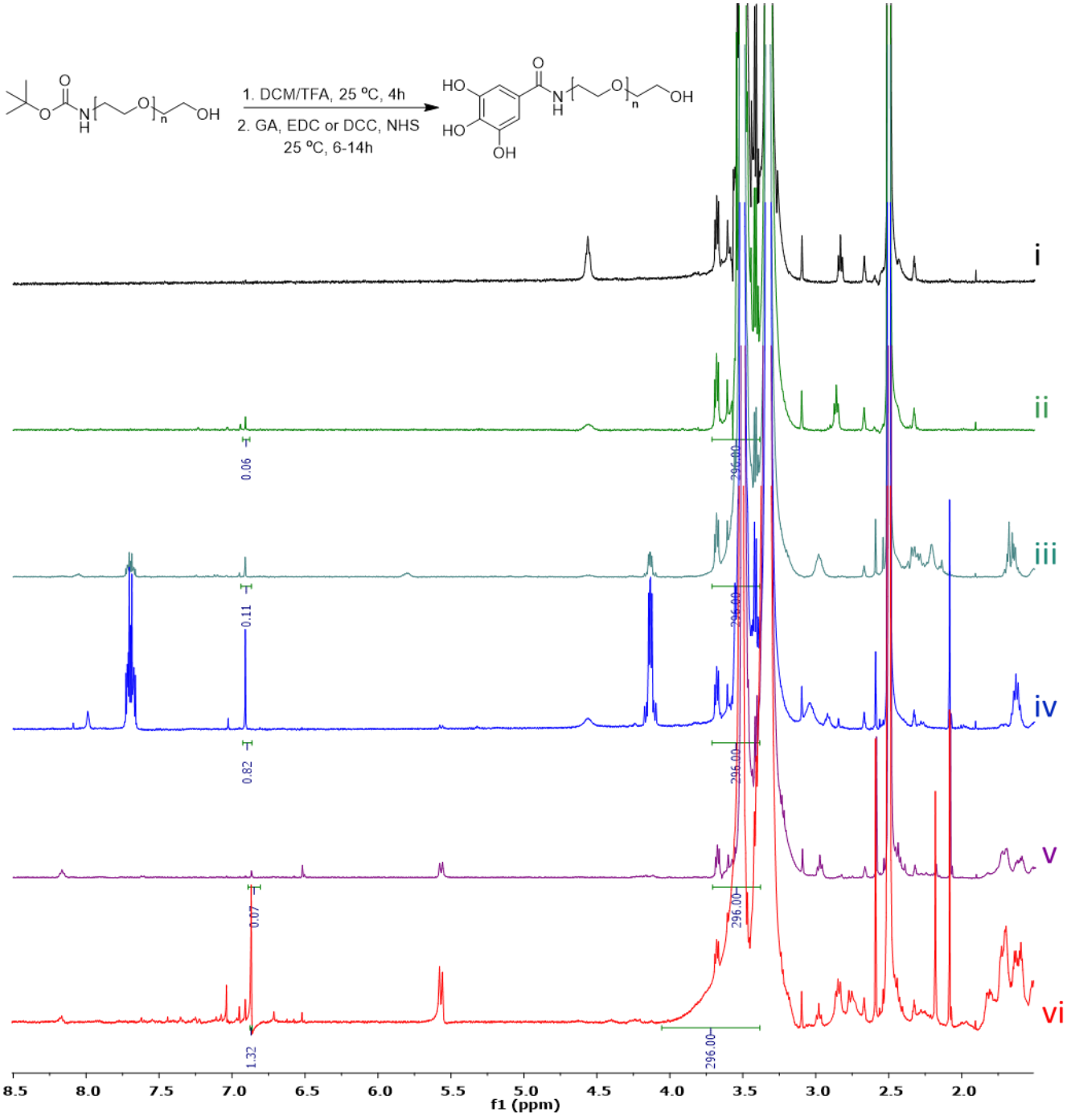

Figure 7. Synthesis of GA-modified PEG and ^{1}H-NMR spectrum of GA conjugated PEG obtained by different reaction conditions in $(CD_3)_2SO$.

Table 3. Synthesis of GA-modified PEG in different reaction conditions and conjugation efficiency corresponded to each condition.

Trial	GA w/v%	NH_2-PEG w/v%	Solvent	Activation reagents	Base	Conjugation conditions	Efficiency %
i	0.5	2	MES pH 6	EDC/NHS	/	6 h	0
ii	1	4	DMSO/MES pH 6	EDC/NHS	/	6 h	3
iii	1	3	DMSO	EDC/NHS	/	14 h under N_2	5.5
iv	0.1	0.3	DMF	EDC/NHS	/	14 h under N_2	41
v	0.2	0.4	THF	DCC/NHS	/	14 h under N_2	3.5
vi	0.2	0.4	THF	DCC/NHS	TEA	14 h under N_2	66

2.4 Conclusion

GA was successfully incorporated into amine-PEG using a similar approach as PBA. However, the conjugation efficiency was much lower than PBA. In addition, GA was prone to oxidation..[93] GA-PEG solutions turned brown during all trials, suggesting GA was oxidized to a quinone. This phenomenon poses a challenge to the storage of GA-functionalized MC as additional precautions are needed to present the oxidation, such as freeze-drying the MC and re-suspending it in the eye drops right before applying it to the eyes. Furthermore, the color change could potentially blur vision. These properties imply that GA might not be an ideal candidate for our intended application.

Chapter III. Targeted MCs through TA-functionalization

3.1 Introduction

TA is a star-shaped polyphenolic acid with five arms. Each arm consists of two GA building blocks. TA is widely found in plants and in fermentation products, such as wine and tea; it exhibits outstanding antioxidant, anticarcinogenic, and antimicrobial properties.[101, 102] In Recent years, an increasing amount of research were focused on utilizing TA, dopamine, and their derivatives in bioadhesive materials. Scientists revealed that mussels are capable to adhere to various surfaces even when the surfaces are wet and turbulent waves constantly hit the mussels. The exceptional features of strong adhesion on wet surfaces and high resistance to shear forces establish TA as an outstanding candidate for ocular drug delivery applications. In this study, the MC consisted of a hydrophilic shell crafted from PEG. The abundant hydrogen bonding sites offered by the ether repeating units of PEG facilitated the crosslinking of TA through hydrogen interactions. In this chapter, I focused on crosslinking TA on PBA-MC to increase the adhesion on the cornea.

3.2 Materials and methods

3.2.1 Materials

TA was purchased from Sigma-Aldrich. The rest of the materials are described in section 1.2.1.

3.2.2 Methods

3.2.2.1 TA coating of PBA-MC

PBA-MC was synthesized using the method mentioned in section 1.1.2, except the vials were placed outside the hood, ensuring overnight stirring. Then, PBA-MC was concentrated with a protein concentrator (MWCO 100kDa) at 2500 rpm and dispersed in 1x PBS with final a concentration of 1 mg/mL. Four glass vials (labeled A-D), each contained 1 mL of the PBA-MC

dispersion and they were stirred at 300 rpm for 5 min to ensure homogeneity. Separately, a series of TA solutions (0.005, 0.01, 0.02 w/v%) was freshly prepared with Mili-Q water. 100 µL of each TA solution was quickly added into vials A-C and 100 µL of Mili-Q water was added into vial D. The dispersion was then stirred for an additional 3 min.

3.2.2.2 DLS and zeta potential measurements

The TA-coated PBA-MCs (TA-PBA-MCs) in 1x PBS were concentrated to 200 µL and redispersed in a total 1 mL of Milli-Q water. Then, the samples were filtered using 0.45 µm filters. DLS and Zeta Potential were measured using the methods mentioned in section 1.1.3.

3.2.2.3 Mucin-targeting effect access via turbidity

The turbidity of mucin solutions mixed with various concentrations of 0.02% TA-PBA-MC was measured using the same methods mentioned in section 1.1.3.

3.3 Results and discussion

TA acid can be crosslinked onto PBA-MC and form a MC with dual mucin-targeting groups. Unfortunately, the amount of TA crosslinked in this experiment was highly limited—we found that if the MC was crosslinked with a TA solution of more than 0.02% (w/v), the MC precipitated. MC concentration and coating pH can significantly influence the results and should be optimized in future works.[103, 104]

3.3.1 DLS, PDI, and zeta potential measurements

DLS, PDI, and zeta potential of TA-PBA-MCs were measured using the same methods described in chapter I (Figure 8). The size of the PBA-MC was measured at 213.3 ± 5.9 nm. The larger size compared to MCs in chapter I is likely due to the slower evaporation rate outside the hood. After

TA coating, the hydrodynamic size of TA-PBA-MCs decreased. 0.005%, 0.01%, and 0.02% TA coating resulted in TA-PBA-MCs with hydrodynamic sizes 169.3 ± 4.8 nm, 149.9 ± 1.9 nm, and 137.7 ± 7.4 nm, respectively. The higher w/v% TA coating led to a smaller MC size. This trend is likely a result of the interaction between TA and PEG. The polyphenol groups in TA can form hydrogen bonds with the ether groups in PEG.[105] As the TA content increases, the five-armed TA molecules interact with more PEG chains and act as crosslinkers between chains. The PEG chains thus pack more densely, resulting in a decrease in size. We also found that the PDI increased after TA-coating compared to that of MCs without TA-coating were below the 0.1 range (Figure 4B). The higher TA% led to higher PDI, indicating TA caused the size of the MCs to become less uniform. Zeta potential of TA-PBA-MCs was measured near zero; there was no significant difference compared to PBA-/NH_2-MCs in chapter I (Figure 4C) or a previous study that utilized MC made of PEG-b-(HPMA-Lac_{m+1}).[1]

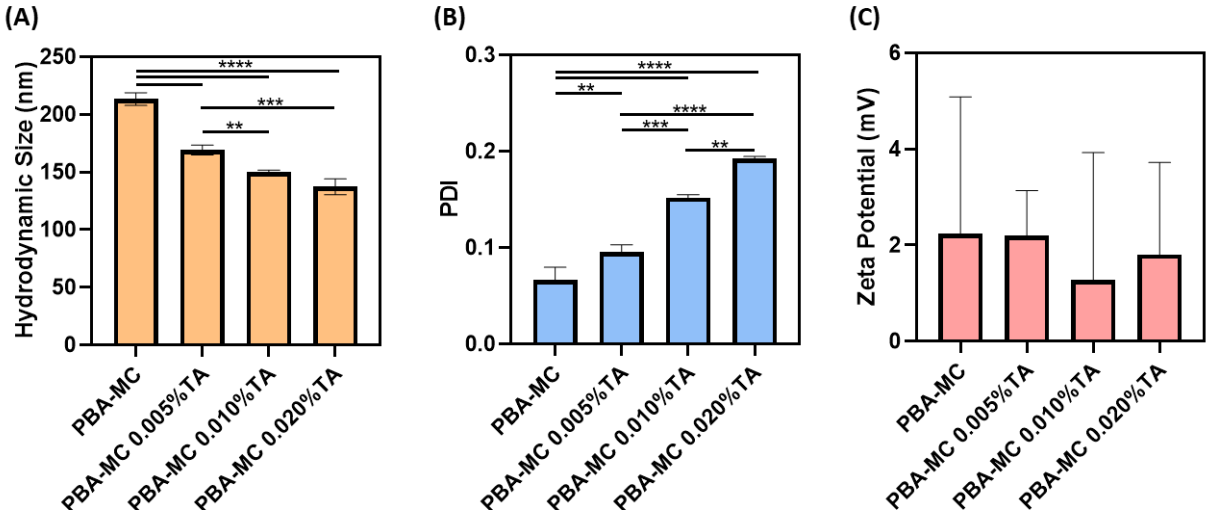

Figure 8. (A) Hydrodynamic size measurements of TA-PBA-MCs; (B) PDI of TA-PBA-MCs obtained by Zetasizer; (C) surface zeta potential measurements of TA-PBA-MCs.

With increasing amounts of TA, a noticeable reduction in the sizes of TA-coated MCs was observed, indicating that TA promotes a denser packing of the PEG shell. This change is likely attributed to the increased hydrogen bonding between TA and PEG chains. Studies have found that polymers formed tighter layers after crosslinking with TA.[104, 106] The compact arrangement of the PEG shell is expected to slow down MC swelling in water and potentially mitigate the initial burst release of encapsulated drugs. Therefore, further investigations are warranted to characterize the drug-releasing profile, which should be explored in future experiments.

3.3.2 Assessment of mucoadhesion via turbidity test

As mentioned in chapter I, section 1.3, mucoadhesive nanoparticles can cause free mucin in a solution to aggregate, which increases the turbidity level of the solution.[79] The turbidity changes of various mucin solutions after mixing with TA-PBA-MCs (with 0.02% TA coating) were measured. As shown in Figure 9, TA-PBA-MC outperformed NH_2-MC and the PBS control on mucoadhesion. However, TA-PBA-MC did not exhibit a better mucoadhesive ability compared to PBA-MC. This was likely because the percentage of TA coated on PBA-MC was too low to make a distinguishing difference.

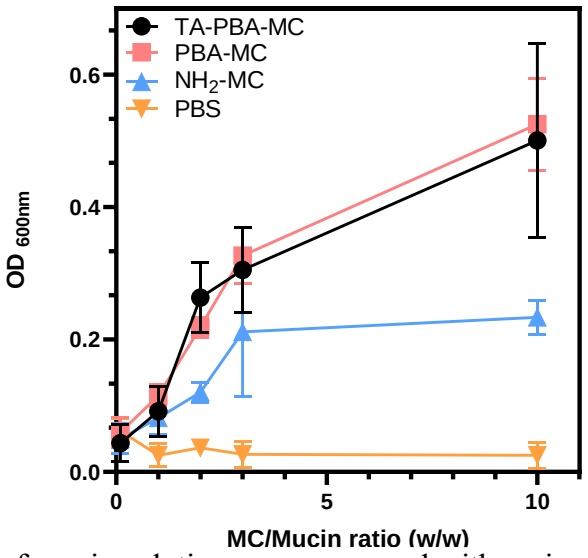

Figure 9. The turbidity of mucin solutions was measured with various MCs to mucin ratios (0.1, 1, 2, 3, 10, w/w%).

3.4 Conclusion

In this chapter, TA was coated on PBA-MC in an attempt to increase the mucoadhesion ability of PBA-MC. The sizes of the TA-coated MCs decreased as the amount of TA increased, likely because TA caused the PEG shell to pack more densely together. A more tightly packed PEG shell could slow down the swelling of MC and potentially reduce the initial burst release of encapsulated drugs. Characterization of the drug-releasing profile should be explored in future experiments. TA-PBA-MC Precipitation of the MC was found in samples coated with TA solutions higher than 0.02% (w/v). This phenomenon greatly limited the coating density of TA on PBA-MC. In the turbidity test, TA-PBA-MC exhibited no distinct difference in mucoadhesion compared to PBA-MC, likely due to the low amount of TA incorporated into the MC. Further optimization on TA-coating density should be explored in future works.

Conclusion

This work developed and functionalized a polymeric micellar drug delivery platform with an ocular-targeting moieties to deliver anti-inflammatory therapeutic, LE. In chapter I, the hydrophobic block of the MC was modified and increased the encapsulation efficiency of LE by over 20%. The MC was found to display a sustained LE-releasing profile for 12 days. Additionally, amine-PEG was used in the hydrophilic block of the MC. The amine functional group is a versatile chemical handle to introduce other moieties onto the MC. PBA was incorporated into the MC through amine-PEG, achieving 91.5% conjugation efficiency. The resulting PBA-MC exhibited excellent adhesion to mucin. PBA-MC can adhere to the corneal mucin without the help of the additional patch. Therefore, the MC drug delivery platform can be formulated into eye drops. The retention on the cornea and the sustained drug release means that the PBA-MC eye drops do not need to be repeatedly re-apply during a short period. Such properties can effectively lower the technical barrier for the patients and improve patient compliance. Furthermore, after a five-day incubation period with PBA-MC, it was observed that human corneal epithelial cells exhibited high cell viability (>95%), along with notable cell spreading and proliferation.

In chapter II, GA was conjugated with the PEG. The conjugation efficiency of GA was suboptimal (66%) compared to PBA. Moreover, GA is susceptible to oxidation, which presents a challenge in terms of storing the GA-functionalized MC. Therefore, GA was not the optimal alternative for PBA for this MC application. In chapter III, TA was coated onto PBA-MC in an attempt to improve mucoadhesion further. The amount of TA that can be coated (0.02%) was too low to make a difference. Thus, PBA-MC was concluded as the best candidate in this study for delivering the anti-inflammatory drug, LE, to the ocular target.

However, there are some limitations to this work. The amine functional group can be used to introduce various moieties onto the MC, and more options should be explored. The EE% of LE was improved in this work, but more hydrophobic drugs should be tested. Additionally, *ex vivo* and *in vivo* experiments are needed in the future to assess the ocular targeting performance of the PBA-MC. In chapter III, TA coating reduced the size of MC; this suggested a more tightly packed PEG shell was formed and it has the potential to mitigate the initial burst release of encapsulated drugs. Additional research is needed to thoroughly examine whether TA or other crosslinkers of PEG could alter the drug-releasing profile.

Supplementary Information

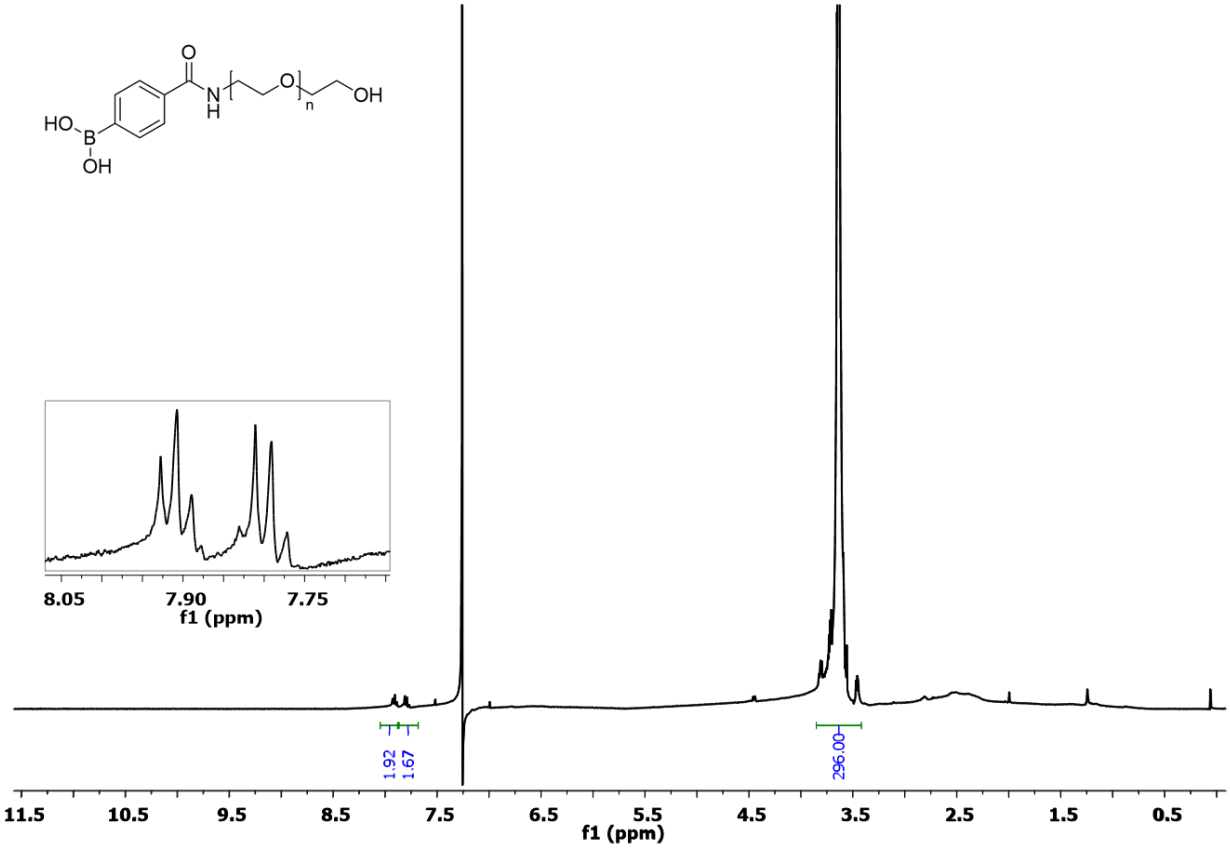

Figure S1. ^{1}H-NMR spectrum of PBA-PEG in $CDCl_3$.

Separation of monomers

The mixture of monomers HPMA-Lac_{m+1} was synthesized using the method described in section 1.1.2.3. Then, the mixture was dissolved in ethyl acetate, mixed with silica gel, loaded in a column, and ran in an automated Isco chromatography system. Solvent A is ethyl acetate and solvent B is hexane. Four different methods were attempted to optimize the separation of HPMA-Lac_{m+1}. Samples eluted out of the silica column chromatography system were collected in a series of test tubes. Thin layer chromatography (TCL) was used to determine which test tubes contained the desirable products. HPMA was used as a reference in TLC. Afterward, the products are condensed with a Rotary evaporator and characterized by ^{1}H NMR spectroscopy.

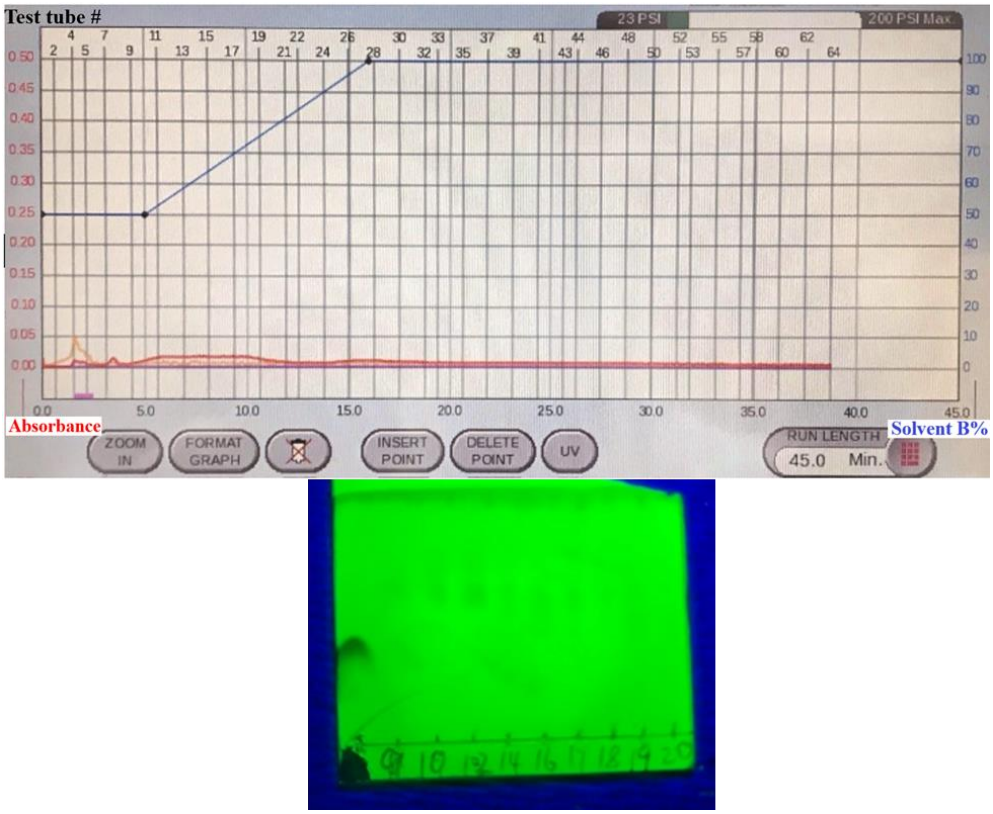

Figure S2. Absorbance peaks of silica column chromatography (top) and signals of TLC (bottom) of method 1.

Method 1

The column was started by calibrating the column with 30% ethyl acetate (0-5 min), followed by raising the up percentage of hexane up to 100% (5-15 min), continuing running the column at 100% hexane (15-40 min). The column was washed with methanol after the run. The absorbance peaks only showed up at the first 5 min of silica column eluent. Signals were only observed at test tubes #9-12 in TLC, corresponding to the samples eluted out of the silica column during the first five minutes (Figure 10). Both results suggested that the products came out too fast and the impurities did not separate well. This indicates the need to decrease the slope of the solvent gradient in order to flush the products out slower and separate them better. There was no obvious

signal in the silica column or TLC after 20 min, indicating that no products or unreacted reagents were rinsed out after 20 min of column running nor during the methanol wash at the end.

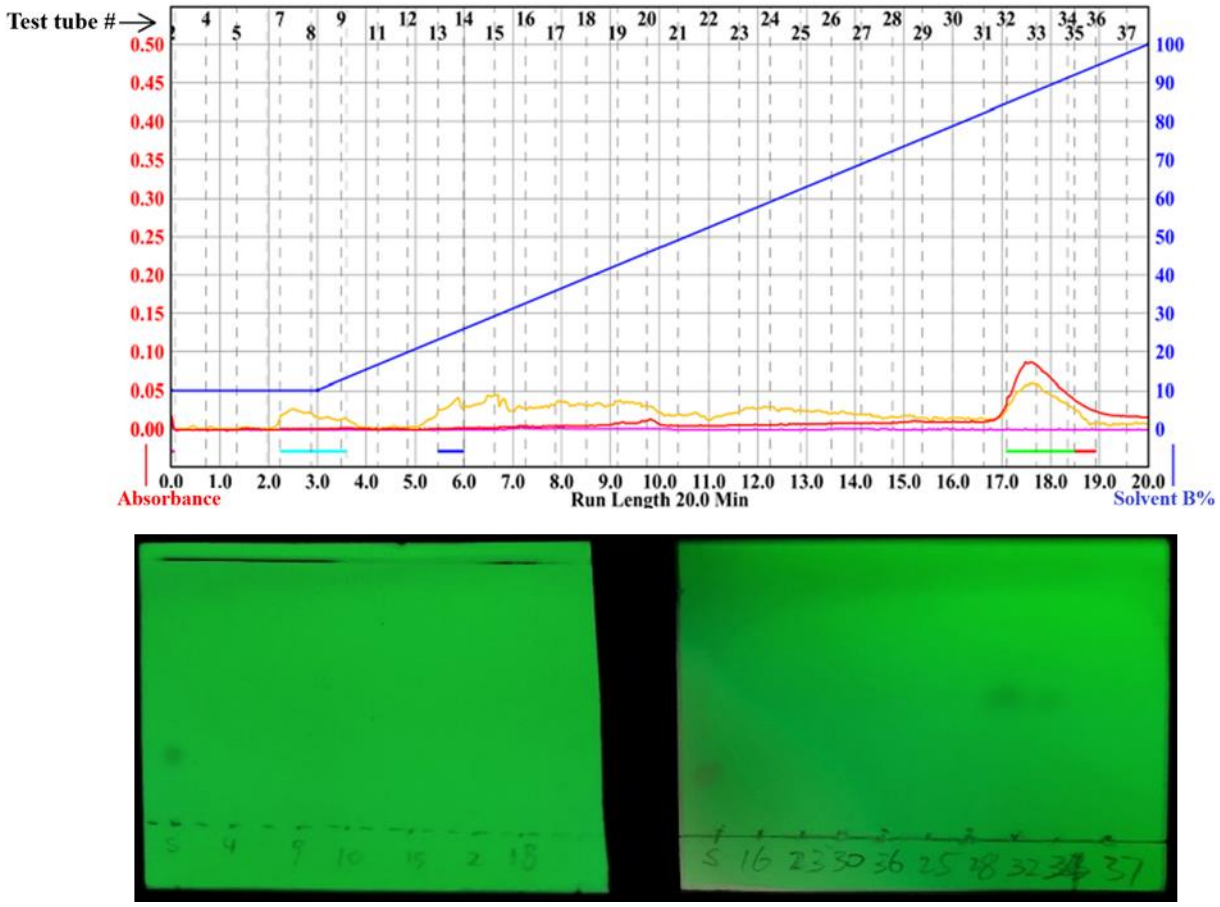

Figure S3. Absorbance peaks of silica column chromatography (top) and signals of TLC (bottom) of method 2.

Method 2

The column was started by calibrating the column with 90% ethyl acetate (0-3 min), followed by raising the percentage of hexane up to 100% (3-20 min). No methanol wash was used.

The absorbance peak measured by the silica column showed at 17-19 min, co-responded to test tube #31-36. There were signals of monomer mixtures shown in TLC at test tubes #32-34 but they were relatively weak (Figure 11). These results suggested that the products came out too slowly.

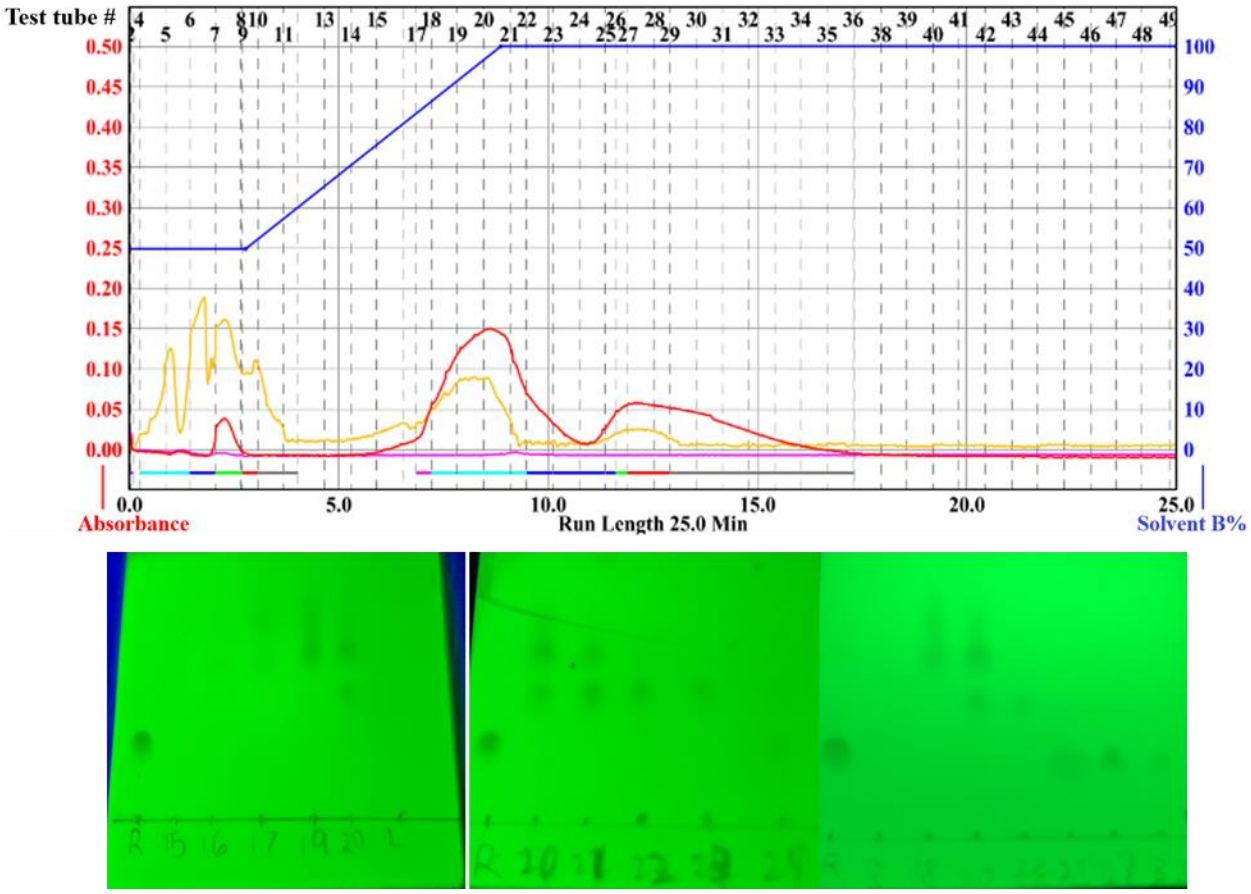

Figure S4. Absorbance peaks of silica column chromatography (top) and signals of TLC (bottom) of method 3.

Method 3

The column was started by calibrating the column with 50% ethyl acetate (0-3 min), followed by raising the up percentage of hexane to 100% (3-9 min), and continue running the column at 100% hexane (9-25 min). No methanol wash was used.

The result is shown in Figure 12. In silica column chromatography, the apparent signal peaks were observed at 6-12 min (co-responded to test tube #16-23) and 12-17 min (co-responded to test tube #24-35). The peak at 6-12 min was relatively narrow, meaning most of the products were eluted out of the silica column in a short time. TLC result showed HPMA was found in tubes # 24-30. HPMA-Lac_{m+1} were found in test tubes #16-23, including HPMA-Lac_2 in #20-23, HPMA-Lac_4 in

#16-21, and HPMA-Lac$_6$ in #16-20. The overlapping of the signals of different monomers indicates the products were not separated well, and a slower change of solvent gradient is needed.

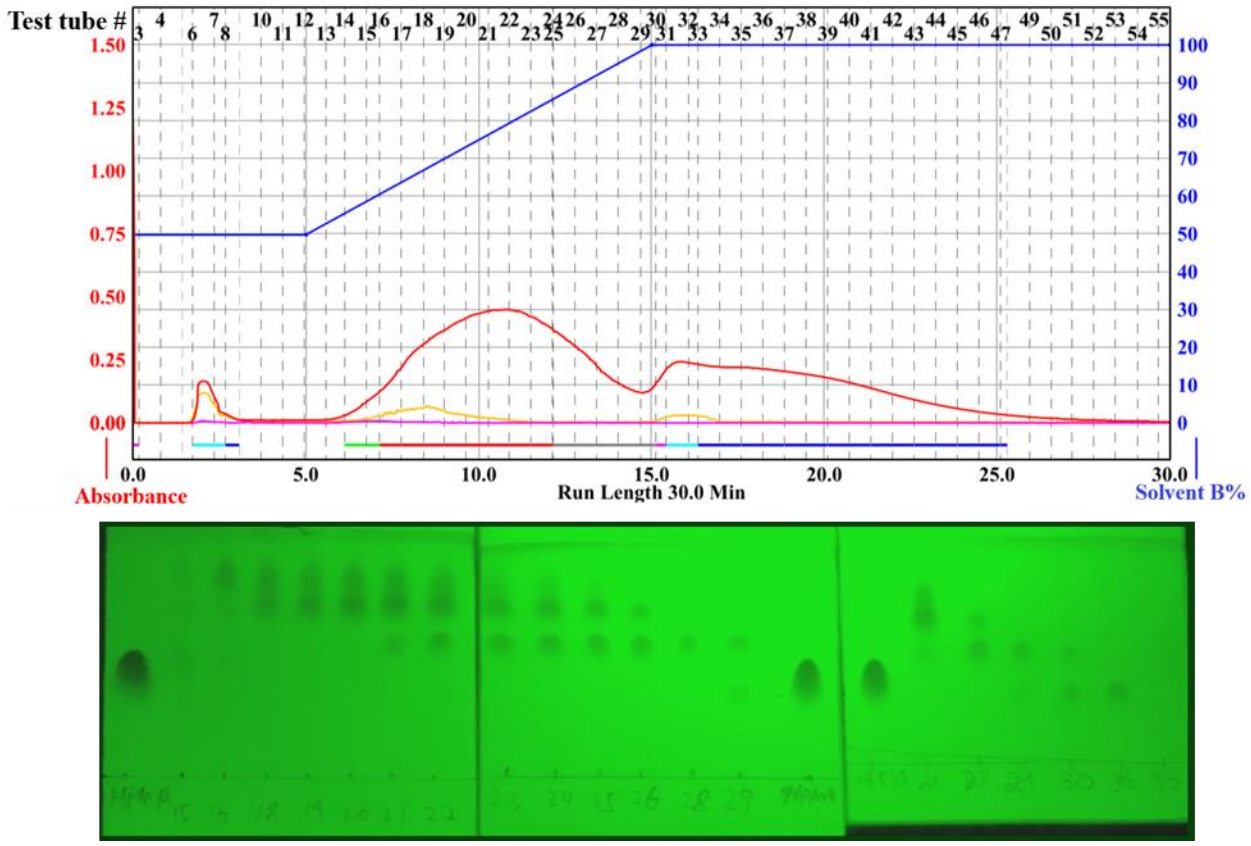

Figure S5. Absorbance peaks of silica column chromatography (top) and signals of TLC (bottom) of method 4.

Method 4

The column was started with 50% ethyl acetate (0-5 min), raised up to 100% (5-15 min), and run at 100% (15-30 min). No methanol wash was used.

Method 4 is the optimized method for separating different HPMA-Lac$_{m+1}$. The obvious signal peaks were observed at 2-3 min (co-responded to test tube #6-7), 6-15 min (co-responded to test tube #14-29), and 15-27 min (co-responded to test tube #30-50) in silica column chromatography. The peak at 6-15 min was much more widely compared to the corresponding peak using method

3, meaning the products were separated better than the samples in method 3. This is because raising the solvent B% gradually increased the separation of monomers with different degrees of hydrophobicity. The unreacted HPMA, which is more hydrophilic than HPMA-Lac_{m+1}, was flushed out of the silica column last due to the highest high affinity to silica gel (tube #30-50). The more Lac repeating units present in a monomer, the more hydrophobic it is, which was expected to be flushed out of the column slower. Due to its hydrophobicity, the unreacted L-lactide was flushed out of the column first (tubes #6-7). Hydrophobic species ran faster in TLC due to the low affinity of these species to the silica board. HPMA was used as a reference. HPMA was found in #29-35. HPMA-Lac_{m+1} monomers were found in test tubes #6-35, including HPMA-Lac_2 in #21-30, HPMA-Lac_4 in #18-26, and HPMA-Lac_6 in #15-22. The separated monomers were characterized by ^{1}H NMR spectroscopy (Figure S6).

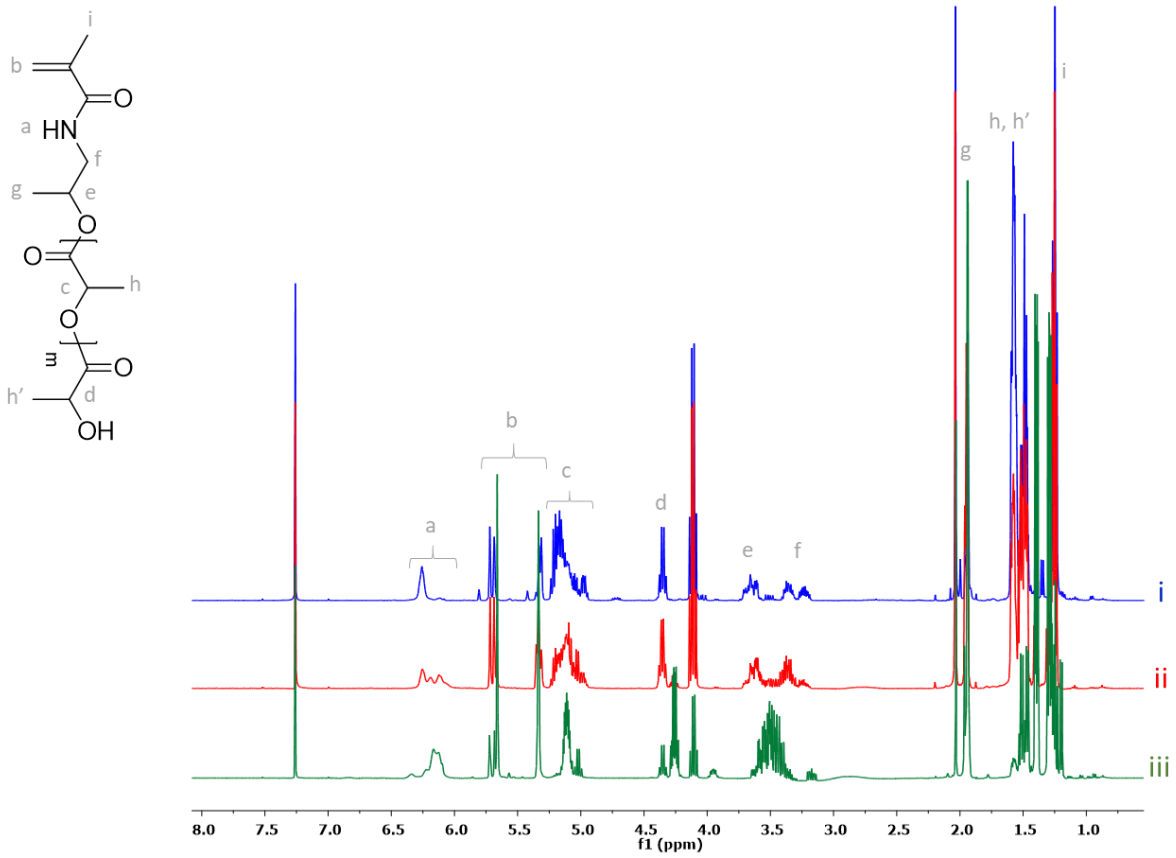

Figure S6. ^{1}H-NMR-spectra of separated HPMA-Lac$_{m+1}$ monomers in $CDCl_3$ (i: m = 5; ii: m = 1, 3, 5; iii: m = 1).

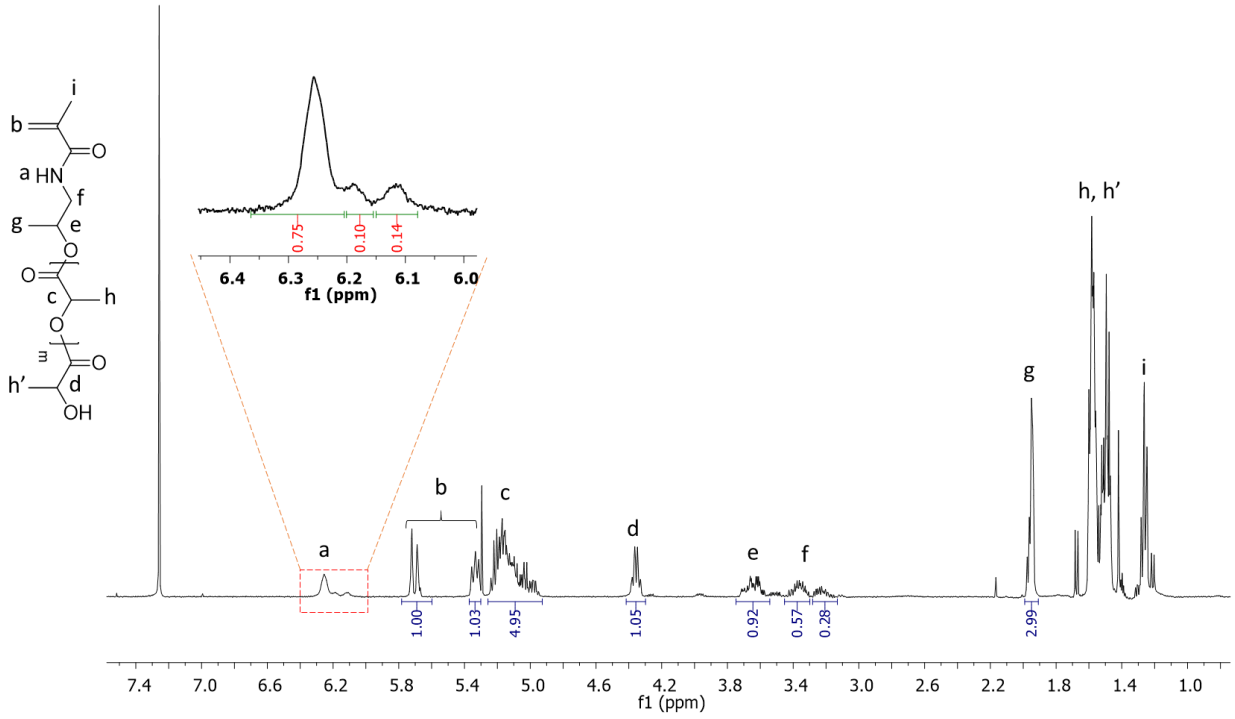

Figure S7. ^{1}H-NMR spectrum of HPMA-Lac$_6$ monomer in $CDCl_3$. obtained by a modified synthesis at 110 °C and reacted for 16 h.

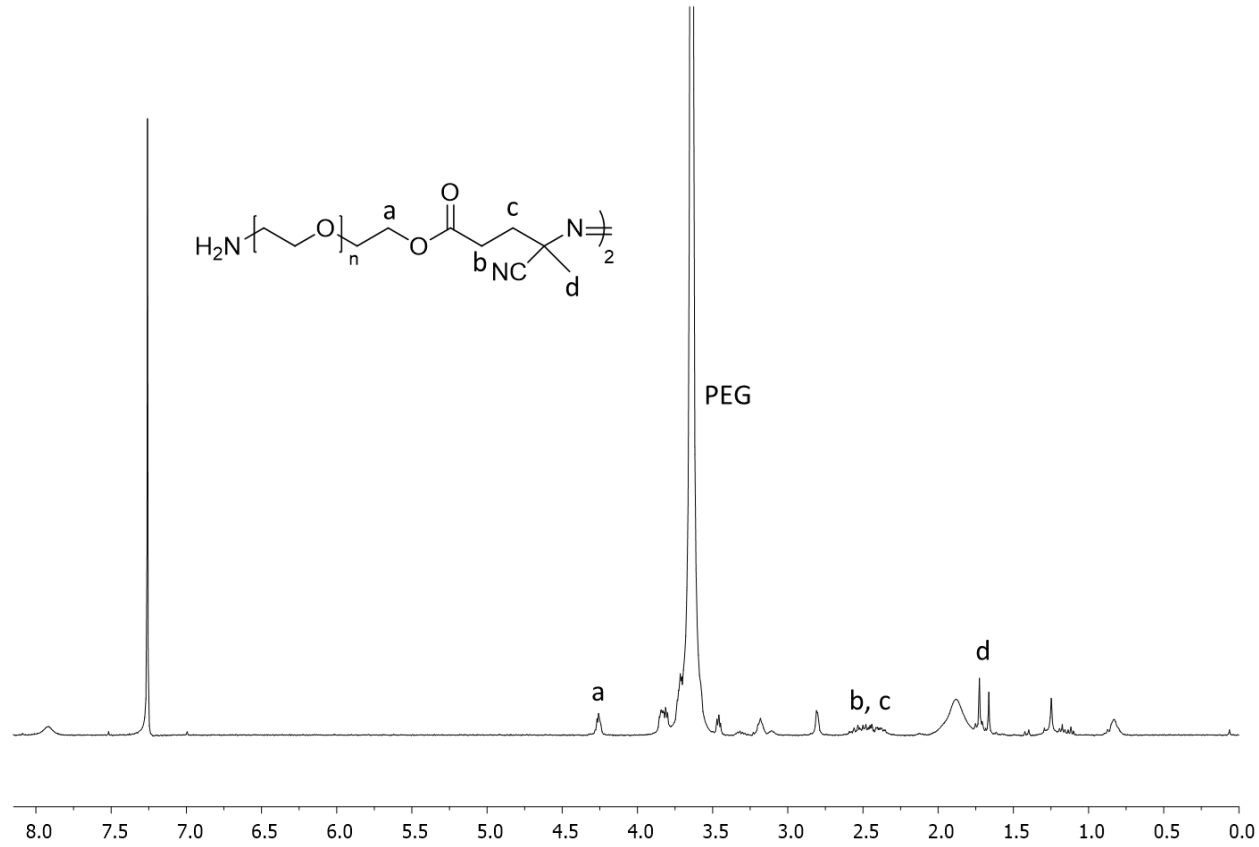

Figure S8. ^{1}H-NMR spectrum of (NH_2-PEG-ACVA) in $CDCl_3$.

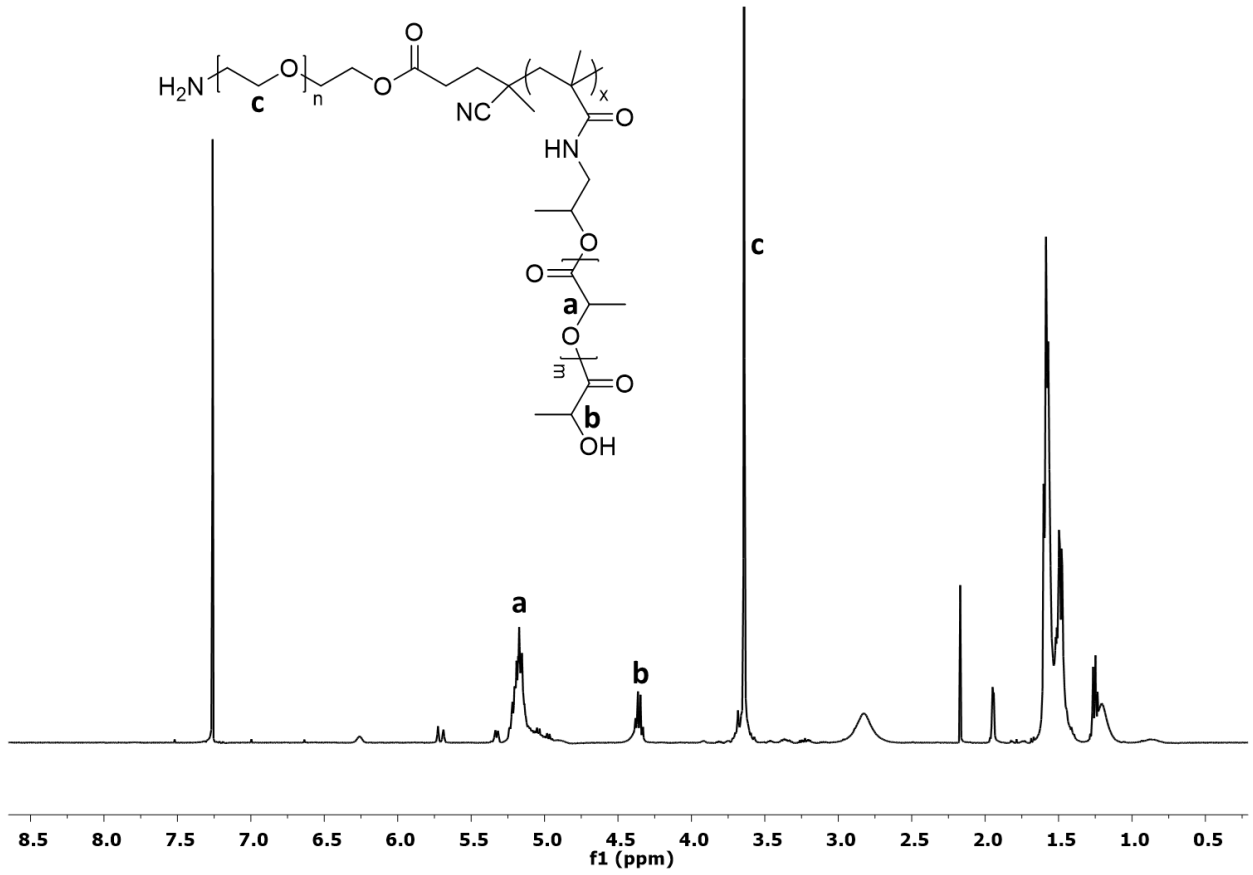

Figure S9. ^{1}H-NMR spectrum of (NH_2-PEG-*b*-(HPMA-Lac_{m+1})) in $CDCl_3$.

(A)

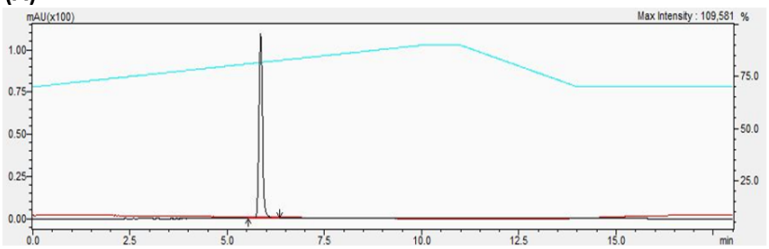

(B)

LE (mg/mL)	Peak Area
0.01	62209
0.02	126411
0.04	251875
0.06	439213
0.08	513082
0.1	699784

(C)

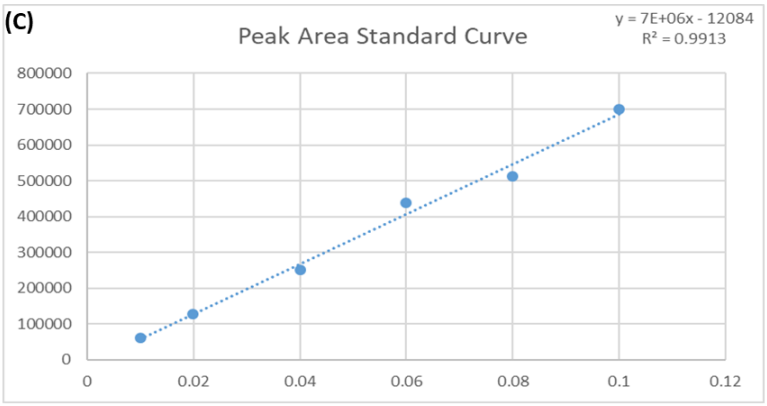

(D)

	Calculated LE (mg/mL)	Peak Area
MC_{lacm+1} (1/10 dilution)	0.077212571	528404
MC_{lac6} (1/10 dilution)	0.053577429	362958

Figure S10. (A) A sample of HPLC measurement of LE concentration (0.06 mg/mL) at 242 nm channel; (B) measured peak areas of samples with known LE concentrations at 242 nm channel using HPLC; (C) plotted LE concentrations vs. measure peak areas and the obtained standard curve function; (D) calculated LE concentrations. After separating the MC-LE supernatant and the unencapsulated LE pellet using centrifugation, the LE pellet was dissolved in 1 mL ACN, and diluted 10 fold. The concentration was measured by HPLC using the same method as the measurements of the standard curve samples. MC_{lacm+1} represents MC formed by copolymer PEG-*b*-(HPMA-Lac_{m+1}), which was synthesized using a mixture of monomers (HPMA-Lac_{m+1}, m=1,3,5). MC_{lac6} represents MC formed by copolymer PEG-*b*-(HPMA-Lac_6), which was synthesized using monomer HPMA-Lac_6.

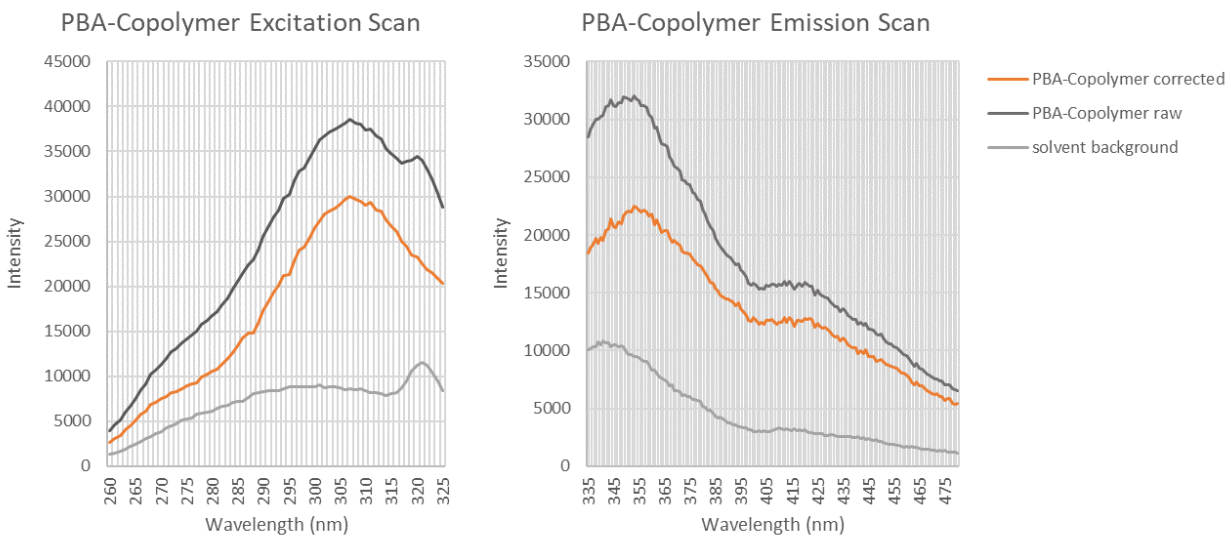

Figure S11. Excitation and emission scan of PBA-copolymer using spectrofluorometer.

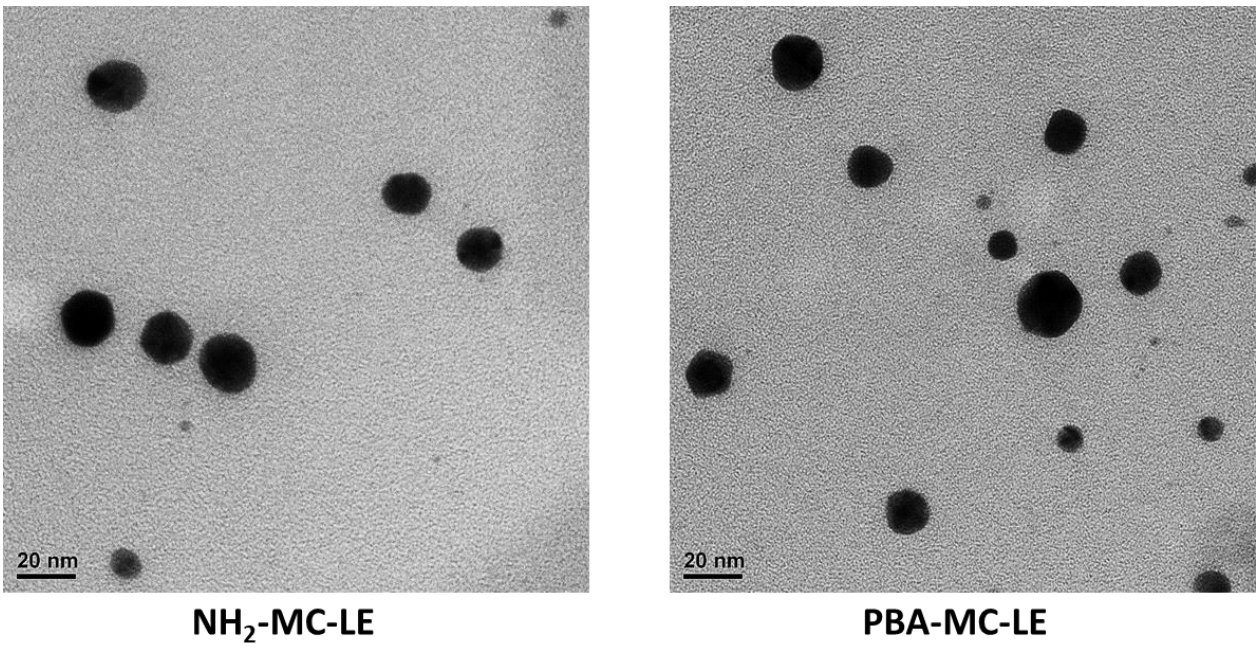

Figure S12. TEM images for PBA-MC-LE and NH_2-MC-LE.

Bibliography

1. Chen, X.; Gholizadeh, S.; Ghovvati, M.; Wang, Z.; Jellen, M. J.; Mostafavi, A.; Dana, R.; Annabi, N. J. A. J., Engineering a drug eluting ocular patch for delivery and sustained release of anti‐inflammatory therapeutics. **2023**, e18067.
2. Lanier, O. L.; Manfre, M. G.; Bailey, C.; Liu, Z.; Sparks, Z.; Kulkarni, S.; Chauhan, A. J. A. P., Review of approaches for increasing ophthalmic bioavailability for eye drop formulations. **2021,** *22*, 1-16.
3. Prosperi-Porta, G.; Kedzior, S.; Muirhead, B.; Sheardown, H., Phenylboronic-Acid-Based Polymeric Micelles for Mucoadhesive Anterior Segment Ocular Drug Delivery. *Biomacromolecules* **2016,** *17* (4), 1449-1457.
4. Liu, S.; Chang, C. N.; Verma, M. S.; Hileeto, D.; Muntz, A.; Stahl, U.; Woods, J.; Jones, L. W.; Gu, F. X. J. N. R., Phenylboronic acid modified mucoadhesive nanoparticle drug carriers facilitate weekly treatment of experimentallyinduced dry eye syndrome. **2015,** *8*, 621-635.
5. Shi, H.; Zhou, J.; Wang, Y.; Zhu, Y.; Lin, D.; Lei, L.; Vakal, S.; Wang, J.; Li, X. J. S., A rapid corneal healing microneedle for efficient ocular drug delivery. **2022,** *18* (4), 2104657.
6. Gadziński, P.; Froelich, A.; Wojtyłko, M.; Białek, A.; Krysztofiak, J.; Osmałek, T. J. B. J. o. N., Microneedle-based ocular drug delivery systems–recent advances and challenges. **2022,** *13* (1), 1167-1184.
7. Mohamdeen, Y. M. G.; Tabriz, A. G.; Tighsazzadeh, M.; Nandi, U.; Khalaj, R.; Andreadis, I.; Boateng, J. S.; Douroumis, D., Development of 3D printed drug-eluting contact lenses. *Journal of Pharmacy and Pharmacology* **2022,** *74* (10), 1467-1476.
8. Alvarez-Lorenzo, C.; Anguiano-Igea, S.; Varela-García, A.; Vivero-Lopez, M.; Concheiro, A. J. A. b., Bioinspired hydrogels for drug-eluting contact lenses. **2019,** *84*, 49-62.
9. Kirchhof, S.; Goepferich, A. M.; Brandl, F. P. J. E. J. o. P.; Biopharmaceutics, Hydrogels in ophthalmic applications. **2015,** *95*, 227-238.
10. Croy, S.; Kwon, G. J. C. p. d., Polymeric micelles for drug delivery. **2006,** *12* (36), 4669-4684.
11. Gholizadeh, S.; Wang, Z.; Chen, X.; Dana, R.; Annabi, N. J. D. D. T., Advanced nanodelivery platforms for topical ophthalmic drug delivery. **2021,** *26* (6), 1437-1449.
12. Tan, G.; Li, J.; Song, Y.; Yu, Y.; Liu, D.; Pan, W., Phenylboronic acid-tethered chondroitin sulfate-based mucoadhesive nanostructured lipid carriers for the treatment of dry eye syndrome. *Acta Biomaterialia* **2019,** *99*, 350-362.
13. Gholizadeh, S.; Wang, Z.; Chen, X.; Dana, R.; Annabi, N., Advanced nanodelivery platforms for topical ophthalmic drug delivery. *Drug Discovery Today* **2021,** *26* (6), 1437-1449.
14. Kolawole, O. M.; Lau, W. M.; Khutoryanskiy, V. V., Synthesis and Evaluation of Boronated Chitosan as a Mucoadhesive Polymer for Intravesical Drug Delivery. *Journal of Pharmaceutical Sciences* **2019,** *108* (9), 3046-3053.
15. Sun, X.; Sheng, Y.; Li, K.; Sai, S.; Feng, J.; Li, Y.; Zhang, J.; Han, J.; Tian, B., Mucoadhesive phenylboronic acid conjugated chitosan oligosaccharide-vitamin E copolymer for topical ocular delivery of voriconazole: Synthesis, in vitro/vivo evaluation, and mechanism. *Acta Biomaterialia* **2022,** *138*, 193-207.
16. Kaldybekov, D. B.; Tonglairoum, P.; Opanasopit, P.; Khutoryanskiy, V. V., Mucoadhesive maleimide-functionalised liposomes for drug delivery to urinary bladder. *European Journal of Pharmaceutical Sciences* **2018,** *111*, 83-90.
17. Kaldybekov, D. B.; Filippov, S. K.; Radulescu, A.; Khutoryanskiy, V. V., Maleimide-functionalised PLGA-PEG nanoparticles as mucoadhesive carriers for intravesical drug delivery. *European Journal of Pharmaceutics and Biopharmaceutics* **2019,** *143*, 24-34.

18. Wu, B.; Sai, S.; Li, K.; Sun, X.; Han, J.; Tian, B., Maleimide-functionalized phospholipid/Pluronic F127 mixed micelles for efficient ophthalmic delivery of voriconazole against Candida albicans. *Colloids and Surfaces B: Biointerfaces* **2022,** *209*, 112180.
19. Fan, Q.-Q.; Zhang, C.-L.; Qiao, J.-B.; Cui, P.-F.; Xing, L.; Oh, Y.-K.; Jiang, H.-L., Extracellular matrix-penetrating nanodrill micelles for liver fibrosis therapy. *Biomaterials* **2020,** *230*, 119616.
20. Shi, H.; van Steenbergen, M. J.; Lou, B.; Liu, Y.; Hennink, W. E.; Kok, R. J., Folate decorated polymeric micelles for targeted delivery of the kinase inhibitor dactolisib to cancer cells. *International Journal of Pharmaceutics* **2020,** *582*, 119305.
21. Liu, Y.; Scrivano, L.; Peterson, J. D.; Fens, M. H. A. M.; Hernández, I. B.; Mesquita, B.; Toraño, J. S.; Hennink, W. E.; van Nostrum, C. F.; Oliveira, S., EGFR-Targeted Nanobody Functionalized Polymeric Micelles Loaded with mTHPC for Selective Photodynamic Therapy. *Molecular Pharmaceutics* **2020,** *17* (4), 1276-1292.
22. Guo, X.; Wang, L.; Duval, K.; Fan, J.; Zhou, S.; Chen, Z. J. A. M., Dimeric drug polymeric micelles with acid‐active tumor targeting and FRET‐traceable drug release. **2018,** *30* (3), 1705436.
23. Miyamoto, T.; Tsuchiya, K.; Numata, K., Endosome-escaping micelle complexes dually equipped with cell-penetrating and endosome-disrupting peptides for efficient DNA delivery into intact plants. *Nanoscale* **2021,** *13* (11), 5679-5692.
24. Albrecht, K.; Bernkop-Schnürch, A., Thiomers: forms, functions and applications to nanomedicine. *Nanomedicine (London, England)* **2007,** *2* (1), 41-50.
25. Mahmood, A.; Lanthaler, M.; Laffleur, F.; Huck, C. W.; Bernkop-Schnürch, A., Thiolated chitosan micelles: Highly mucoadhesive drug carriers. *Carbohydrate Polymers* **2017,** *167*, 250-258.
26. Gorantla, S.; Rapalli, V. K.; Waghule, T.; Singh, P. P.; Dubey, S. K.; Saha, R. N.; Singhvi, G. J. R. a., Nanocarriers for ocular drug delivery: Current status and translational opportunity. **2020,** *10* (46), 27835-27855.
27. Rozi, M. F.; Sabere, A. S. M. J. J. o. P., A Review on Conventional and Novel Topical Ocular Drug Delivery System. **2021,** *1* (1), 19-26.
28. Ensign, L. M.; Cone, R.; Hanes, J. J. A. d. d. r., Oral drug delivery with polymeric nanoparticles: the gastrointestinal mucus barriers. **2012,** *64* (6), 557-570.
29. Managuli, R. S.; Raut, S. Y.; Reddy, M. S.; Mutalik, S. J. E. o. o. d. d., Targeting the intestinal lymphatic system: a versatile path for enhanced oral bioavailability of drugs. **2018,** *15* (8), 787-804.
30. Vedadghavami, A.; Zhang, C.; Bajpayee, A. G. J. N. t., Overcoming negatively charged tissue barriers: Drug delivery using cationic peptides and proteins. **2020,** *34*, 100898.
31. Guan, J.; Zhou, Z.-Q.; Chen, M.-H.; Li, H.-Y.; Tong, D.-N.; Yang, J.; Yao, J.; Zhang, Z.-Y., Folate-conjugated and pH-responsive polymeric micelles for target-cell-specific anticancer drug delivery. *Acta Biomaterialia* **2017,** *60*, 244-255.
32. Sánchez, A.; Pedroso, E.; Grandas, A., Maleimide-Dimethylfuran exo Adducts: Effective Maleimide Protection in the Synthesis of Oligonucleotide Conjugates. *Organic Letters* **2011,** *13* (16), 4364-4367.
33. Hock, N.; Racaniello, G. F.; Aspinall, S.; Denora, N.; Khutoryanskiy, V. V.; Bernkop‐Schnürch, A. J. A. S., Thiolated nanoparticles for biomedical applications: mimicking the workhorses of our body. **2022,** *9* (1), 2102451.
34. Bernardini, R.; Oliva, A.; Paganelli, A.; Menta, E.; Grugni, M.; Munari, S. D.; Goldoni, L. J. C. l., Stability of boronic esters to hydrolysis: a comparative study. **2009,** *38* (7), 750-751.
35. Huang, Y.; He, Y.; Xia, X.; Quan, H.; Yu, J., Phenylboronic acid-functionalized co-delivery micelles with synergistic effect and down-regulation of HIF-1alpha to overcome multidrug resistance. *Journal of Drug Delivery Science and Technology* **2021,** *62*, 102346.

36. Zhang, L.; Shi, D.; Gao, Y.; Zhou, T.; Chen, M., Phenylboronic acid-functionalized unimolecular micelles based on a star polyphosphoester random copolymer for tumor-targeted drug delivery. *Polymer Chemistry* **2020,** *11* (12), 2252-2261.
37. Tiwari, S.; Sarolia, J.; Kansara, V.; Chudasama, N. A.; Prasad, K.; Ray, D.; Aswal, V. K.; Bahadur, P., Synthesis, Colloidal Characterization and Targetability of Phenylboronic Acid Functionalized α-Tocopheryl Polyethylene Glycol Succinate in Cancer Cells. *Polymers* **2020,** *12* (10).
38. Huang, Q.; Wang, L.; Yu, H.; Ur-Rahman, K., Advances in phenylboronic acid-based closed-loop smart drug delivery system for diabetic therapy. *Journal of Controlled Release* **2019,** *305*, 50-64.
39. Jamard, M.; Sheardown, H., Effect of Methylcellulose Molecular Weight on the Properties of Self-Assembling MC-g-PNtBAm Nanogels. *Bioengineering* **2018,** *5*, 39.
40. Jamard, M.; Sheardown, H., Phenylboronic acid functionalized methylcellulose based nanogels as mucoadhesive ocular drug delivery system. *Frontiers in Bioengineering and Biotechnology* **2016,** *4*.
41. Soga, O.; van Nostrum, C. F.; Ramzi, A.; Visser, T.; Soulimani, F.; Frederik, P. M.; Bomans, P. H. H.; Hennink, W. E., Physicochemical Characterization of Degradable Thermosensitive Polymeric Micelles. *Langmuir* **2004,** *20* (21), 9388-9395.
42. Liu, G.-Y.; Chen, C.-J.; Ji, J. J. S. M., Biocompatible and biodegradable polymersomes as delivery vehicles in biomedical applications. **2012,** *8* (34), 8811-8821.
43. Chen, W.; Zhou, S.; Ge, L.; Wu, W.; Jiang, X. J. B., Translatable high drug loading drug delivery systems based on biocompatible polymer nanocarriers. **2018,** *19* (6), 1732-1745.
44. van Dijk-Wolthuls, W. N. E.; Tsang, S. K. Y.; Kettenes-van den BoschW.E. Hennink, J. J., A new class of polymerizable dextrans with hydrolyzable groups: hydroxyethyl methacrylated dextran with and without oligolactate spacer. *Polymer* **1997,** *38* (25), 6235-6242.
45. Soga, O.; van Nostrum, C. F.; Hennink, W. E., Poly(N-(2-hydroxypropyl) Methacrylamide Mono/Di Lactate): A New Class of Biodegradable Polymers with Tuneable Thermosensitivity. *Biomacromolecules* **2004,** *5* (3), 818-821.
46. Feng, L.; Mumper, R. J. J. C. l., A critical review of lipid-based nanoparticles for taxane delivery. **2013,** *334* (2), 157-175.
47. Önyüksel, H.; Jeon, E.; Rubinstein, I. J. C. l., Nanomicellar paclitaxel increases cytotoxicity of multidrug resistant breast cancer cells. **2009,** *274* (2), 327-330.
48. Lu, Y.; Zhang, E.; Yang, J.; Cao, Z., Strategies to improve micelle stability for drug delivery. *Nano Res* **2018,** *11* (10), 4985-4998.
49. Zhang, X.; Wu, Y.; Zhang, M.; Mao, J.; Wu, Y.; Zhang, Y.; Yao, J.; Xu, C.; Guo, W.; Yu, B. J. I. J. o. N., Sodium cholate-enhanced polymeric micelle system for tumor-targeting delivery of paclitaxel. **2017,** *12*, 8779.
50. Song, X.; Zhao, Y.; Wu, W.; Bi, Y.; Cai, Z.; Chen, Q.; Li, Y.; Hou, S., PLGA nanoparticles simultaneously loaded with vincristine sulfate and verapamil hydrochloride: Systematic study of particle size and drug entrapment efficiency. *International Journal of Pharmaceutics* **2008,** *350* (1), 320-329.
51. Song, X.; Zhao, Y.; Hou, S.; Xu, F.; Zhao, R.; He, J.; Cai, Z.; Li, Y.; Chen, Q., Dual agents loaded PLGA nanoparticles: Systematic study of particle size and drug entrapment efficiency. *European Journal of Pharmaceutics and Biopharmaceutics* **2008,** *69* (2), 445-453.
52. Vanparijs, N.; Maji, S.; Louage, B.; Voorhaar, L.; Laplace, D.; Zhang, Q.; Shi, Y.; Hennink, W. E.; Hoogenboom, R.; De Geest, B. J. P. C., Polymer-protein conjugation via a 'grafting to'approach–a comparative study of the performance of protein-reactive RAFT chain transfer agents. **2015,** *6* (31), 5602-5614.
53. Han, K.; Woghiren, O. E.; Priefer, R. J. C. C. J., Surface tension examination of various liquid oral, nasal, and ophthalmic dosage forms. **2016,** *10* (1), 1-5.
54. Simmons, P. A.; Vehige, J. G. J. C. O., Investigating the potential benefits of a new artificial tear formulation combining two polymers. **2017**, 1637-1642.

55. Gagliano, C.; Papa, V.; Amato, R.; Malaguarnera, G.; Avitabile, T. J. C. E. R., Measurement of the retention time of different ophthalmic formulations with ultrahigh-resolution optical coherence tomography. **2018,** *43* (4), 499-502.
56. Oechsner, M.; Keipert, S. J. E. j. o. p.; biopharmaceutics, Polyacrylic acid/polyvinylpyrrolidone bipolymeric systems. I. Rheological and mucoadhesive properties of formulations potentially useful for the treatment of dry-eye-syndrome. **1999,** *47* (2), 113-118.
57. Wang, C.; Yan, Q.; Liu, H.-B.; Zhou, X.-H.; Xiao, S.-J., Different EDC/NHS Activation Mechanisms between PAA and PMAA Brushes and the Following Amidation Reactions. *Langmuir* **2011,** *27* (19), 12058-12068.
58. D'Este, M.; Eglin, D.; Alini, M., A systematic analysis of DMTMM vs EDC/NHS for ligation of amines to Hyaluronan in water. *Carbohydrate Polymers* **2014,** *108*, 239-246.
59. Fischer, M. J. E., Amine Coupling Through EDC/NHS: A Practical Approach. In *Surface Plasmon Resonance: Methods and Protocols*, Mol, N. J.; Fischer, M. J. E., Eds. Humana Press: Totowa, NJ, 2010; pp 55-73.
60. Zhu, D.; Miao, Z. Y.; Hu, Y.; Zhang, X. J., Single-step, homogeneous and sensitive detection for microRNAs with dual-recognition steps based on luminescence resonance energy transfer (LRET) using upconversion nanoparticles. *Biosensors and Bioelectronics* **2018,** *100*, 475-481.
61. Chung, D.-J.; Oh, S.-H.; Komathi, S.; Gopalan, A. I.; Lee, K.-P.; Choi, S.-H., One-step modification of various electrode surfaces using diazonium salt compounds and the application of this technology to electrochemical DNA (E-DNA) sensors. *Electrochimica Acta* **2012,** *76*, 394-403.
62. Bartczak, D.; Kanaras, A. G., Preparation of Peptide-Functionalized Gold Nanoparticles Using One Pot EDC/Sulfo-NHS Coupling. *Langmuir* **2011,** *27* (16), 10119-10123.
63. Wissink, M. J. B.; Beernink, R.; Pieper, J. S.; Poot, A. A.; Engbers, G. H. M.; Beugeling, T.; van Aken, W. G.; Feijen, J., Immobilization of heparin to EDC/NHS-crosslinked collagen. Characterization and in vitro evaluation. *Biomaterials* **2001,** *22* (2), 151-163.
64. Lee, J.; Edwards, H.; Pereira, C.; Samii, S. J. J. o. M. S. M. i. M., Crosslinking of tissue-derived biomaterials in 1-ethyl-3-(3-dimethylaminopropyl)-carbodiimide (EDC). **1996,** *7* (9), 531-541.
65. Nakajima, N.; Ikada, Y., Mechanism of Amide Formation by Carbodiimide for Bioconjugation in Aqueous Media. *Bioconjugate Chemistry* **1995,** *6* (1), 123-130.
66. Gee, N. PH for EDC/NHS coupling. https://www.researchgate.net/post/PH_for_EDC_NHS_coupling.
67. Bulpitt, P.; Aeschlimann, D. J. J. o. b. m. r., New strategy for chemical modification of hyaluronic acid: preparation of functionalized derivatives and their use in the formation of novel biocompatible hydrogels. **1999,** *47* (2), 152-169.
68. Pieper, J. S.; Hafmans, T.; Veerkamp, J. H.; van Kuppevelt, T. H., Development of tailor-made collagen–glycosaminoglycan matrices: EDC/NHS crosslinking, and ultrastructural aspects. *Biomaterials* **2000,** *21* (6), 581-593.
69. Puertas, S.; de Gracia Villa, M.; Mendoza, E.; Jiménez-Jorquera, C.; de la Fuente, J. M.; Fernández-Sánchez, C.; Grazú, V., Improving immunosensor performance through oriented immobilization of antibodies on carbon nanotube composite surfaces. *Biosensors and Bioelectronics* **2013,** *43*, 274-280.
70. Yang, C., Enhanced physicochemical properties of collagen by using EDC/NHS-crosslinking. *Bulletin of Materials Science* **2012,** *35* (5), 913-918.
71. Gratzer, P. F.; Lee, J. M. J. J. o. B. M. R. A. O. J. o. T. S. f. B., The Japanese Society for Biomaterials,; Biomaterials, T. A. S. f.; Biomaterials, t. K. S. f., Control of pH alters the type of cross‐linking produced by 1‐ethyl‐3‐(3‐dimethylaminopropyl)‐carbodiimide (EDC) treatment of acellular matrix vascular grafts. **2001,** *58* (2), 172-179.

72. Soga, O.; van Nostrum, C. F.; Fens, M.; Rijcken, C. J.; Schiffelers, R. M.; Storm, G.; Hennink, W. E. J. J. o. C. R., Thermosensitive and biodegradable polymeric micelles for paclitaxel delivery. **2005,** *103* (2), 341-353.
73. Riley, T.; Stolnik, S.; Heald, C. R.; Xiong, C. D.; Garnett, M. C.; Illum, L.; Davis, S. S.; Purkiss, S. C.; Barlow, R. J.; Gellert, P. R., Physicochemical Evaluation of Nanoparticles Assembled from Poly(lactic acid)−Poly(ethylene glycol) (PLA−PEG) Block Copolymers as Drug Delivery Vehicles. *Langmuir* **2001,** *17* (11), 3168-3174.
74. Powell, C. H., Stanley Ophthalmic solution. **2005**.
75. Dave, R. S.; Goostrey, T. C.; Ziolkowska, M.; Czerny-Holownia, S.; Hoare, T.; Sheardown, H., Ocular drug delivery to the anterior segment using nanocarriers: A mucoadhesive/mucopenetrative perspective. *Journal of Controlled Release* **2021,** *336*, 71-88.
76. Xia, X.; Yang, M.; Wang, Y.; Zheng, Y.; Li, Q.; Chen, J.; Xia, Y., Quantifying the coverage density of poly(ethylene glycol) chains on the surface of gold nanostructures. *ACS Nano* **2012,** *6* (1), 512-22.
77. Li, L. D.; Crouzier, T.; Sarkar, A.; Dunphy, L.; Han, J.; Ribbeck, K., Spatial configuration and composition of charge modulates transport into a mucin hydrogel barrier. *Biophysical journal* **2013,** *105* (6), 1357-65.
78. Hodges, R. R.; Dartt, D. A., Tear film mucins: Front line defenders of the ocular surface; comparison with airway and gastrointestinal tract mucins. *Experimental Eye Research* **2013,** *117*, 62-78.
79. Shin, M.; Kim, K.; Shim, W.; Yang, J. W.; Lee, H. J. A. B. S.; Engineering, Tannic acid as a degradable mucoadhesive compound. **2016,** *2* (4), 687-696.
80. Guzman-Aranguez, A.; Argüeso, P., Structure and Biological Roles of Mucin-type O-glycans at the Ocular Surface. *The Ocular Surface* **2010,** *8* (1), 8-17.
81. Wang, D.-E.; Yan, J.; Jiang, J.; Liu, X.; Tian, C.; Xu, J.; Yuan, M.-S.; Han, X.; Wang, J. J. N., Polydiacetylene liposomes with phenylboronic acid tags: a fluorescence turn-on sensor for sialic acid detection and cell-surface glycan imaging. **2018,** *10* (9), 4570-4578.
82. Liu, S.; Dozois, M. D.; Chang, C. N.; Ahmad, A.; Ng, D. L. T.; Hileeto, D.; Liang, H.; Reyad, M.-M.; Boyd, S.; Jones, L. W.; Gu, F. X., Prolonged Ocular Retention of Mucoadhesive Nanoparticle Eye Drop Formulation Enables Treatment of Eye Diseases Using Significantly Reduced Dosage. *Molecular Pharmaceutics* **2016,** *13* (9), 2897-2905.
83. Zhou, J.; Wang, R.; Su, W.; Zhang, L.; Li, A.; Jiao, T., Efficient detection of glucose by graphene-based non-enzymatic sensing material based on carbon dot. *Colloids and Surfaces A: Physicochemical and Engineering Aspects* **2022,** *647*, 129122.
84. Deshayes, S.; Cabral, H.; Ishii, T.; Miura, Y.; Kobayashi, S.; Yamashita, T.; Matsumoto, A.; Miyahara, Y.; Nishiyama, N.; Kataoka, K., Phenylboronic Acid-Installed Polymeric Micelles for Targeting Sialylated Epitopes in Solid Tumors. *Journal of the American Chemical Society* **2013,** *135* (41), 15501-15507.
85. Badhani, B.; Sharma, N.; Kakkar, R. J. R. A., Gallic acid: A versatile antioxidant with promising therapeutic and industrial applications. **2015,** *5* (35), 27540-27557.
86. Rivera‐Pastrana, D. M.; Yahia, E. M.; González‐Aguilar, G. A. J. J. o. t. S. o. F.; Agriculture, Phenolic and carotenoid profiles of papaya fruit (Carica papaya L.) and their contents under low temperature storage. **2010,** *90* (14), 2358-2365.
87. Choubey, S.; Goyal, S.; Varughese, L. R.; Kumar, V.; Sharma, A. K.; Beniwal, V. J. M. r. i. m. c., Probing gallic acid for its broad spectrum applications. **2018,** *18* (15), 1283-1293.
88. Kahkeshani, N.; Farzaei, F.; Fotouhi, M.; Alavi, S. S.; Bahramsoltani, R.; Naseri, R.; Momtaz, S.; Abbasabadi, Z.; Rahimi, R.; Farzaei, M. H. J. I. j. o. b. m. s., Pharmacological effects of gallic acid in health and diseases: A mechanistic review. **2019,** *22* (3), 225.
89. Kord Forooshani, P.; Lee, B. P. J. J. o. P. S. P. A. P. C., Recent approaches in designing bioadhesive materials inspired by mussel adhesive protein. **2017,** *55* (1), 9-33.

90. Ramirez-Barron, S. N.; Sanchez-Valdes, S.; Betancourt, R.; Gallardo, C. A.; Puente-Urbina, B.; Rodriguez-Fernández, O. S.; Carneiro-da Cunha, M. G.; dos Santos- Correia, M. T.; Sanchez-Martinez, Z. V., Preparation and characterization of gelatin-gallic acid/ZnO nanocomposite with antibacterial properties as a promising multi-functional bioadhesive for wound dressing applications. *International Journal of Adhesion and Adhesives* **2021,** *104*, 102749.
91. Yu, L.; Luo, Z.; Chen, T.; Ouyang, Y.; Xiao, L.; Liang, S.; Peng, Z.; Liu, Y.; Deng, Y., Bioadhesive Nanoparticles for Local Drug Delivery. **2022,** *23* (4), 2370.
92. López-Martínez, L. M.; Santacruz-Ortega, H.; Navarro, R.-E.; Sotelo-Mundo, R. R.; González-Aguilar, G. A. J. P. o., A 1H NMR investigation of the interaction between phenolic acids found in mango (Manguifera indica cv Ataulfo) and papaya (Carica papaya cv Maradol) and 1, 1-diphenyl-2-picrylhydrazyl (DPPH) free radicals. **2015,** *10* (11), e0140242.
93. Friedman, M.; Jürgens, H. S., Effect of pH on the Stability of Plant Phenolic Compounds. *Journal of Agricultural and Food Chemistry* **2000,** *48* (6), 2101-2110.
94. Heravi, M. M.; Ghavidel, M.; Mohammadkhani, L. J. R. a., Beyond a solvent: triple roles of dimethylformamide in organic chemistry. **2018,** *8* (49), 27832-27862.
95. Liu, S.-Q.; Wiradharma, N.; Gao, S.-J.; Tong, Y. W.; Yang, Y.-Y., Bio-functional micelles self-assembled from a folate-conjugated block copolymer for targeted intracellular delivery of anticancer drugs. *Biomaterials* **2007,** *28* (7), 1423-1433.
96. Zhang, Z.; Cai, R.; Long, F.; Wang, J., Development and application of tetrabromobisphenol A imprinted electrochemical sensor based on graphene/carbon nanotubes three-dimensional nanocomposites modified carbon electrode. *Talanta* **2015,** *134*, 435-442.
97. Li, J.; Yoong, S. L.; Goh, W. J.; Czarny, B.; Yang, Z.; Poddar, K.; Dykas, M. M.; Patra, A.; Venkatesan, T.; Panczyk, T.; Lee, C.; Pastorin, G., In vitro controlled release of cisplatin from gold-carbon nanobottles via cleavable linkages. *Int J Nanomedicine* **2015,** *10*, 7425-41.
98. Burke, R. S.; Pun, S. H., Extracellular Barriers to in Vivo PEI and PEGylated PEI Polyplex-Mediated Gene Delivery to the Liver. *Bioconjugate Chemistry* **2008,** *19* (3), 693-704.
99. Wu, J.; Liu, Q.; Lee, R. J., A folate receptor-targeted liposomal formulation for paclitaxel. *International Journal of Pharmaceutics* **2006,** *316* (1), 148-153.
100. Wang, J. H.; Eychenne, R.; Wolff, M.; Mallet‐Ladeira, S.; Lepareur, N.; Benoist, E. J. E. J. o. I. C., Design, synthesis, and reactivity of multidentate ligands with Rhenium (I) and Rhenium (V) Cores. **2017,** *2017* (33), 3908-3918.
101. Baldwin, A.; Booth, B. W. J. J. o. B. A., Biomedical applications of tannic acid. **2022,** *36* (8), 1503-1523.
102. Kaczmarek, B. J. M., Tannic acid with antiviral and antibacterial activity as a promising component of biomaterials—A minireview. **2020,** *13* (14), 3224.
103. Huang, H.; Li, P.; Liu, C.; Ma, H.; Huang, H.; Lin, Y.; Wang, C.; Yang, Y. J. R. a., pH-Responsive nanodrug encapsulated by tannic acid complex for controlled drug delivery. **2017,** *7* (5), 2829-2835.
104. Li, R.; Peng, S.; Zhang, R.; Dai, T.; Fu, G.; Wan, Y.; Liu, C.; McClements, D. J., Formation and characterization of oil-in-water emulsions stabilized by polyphenol-polysaccharide complexes: Tannic acid and β-glucan. *Food Research International* **2019,** *123*, 266-275.
105. Shin, M.; Kim, K.; Shim, W.; Yang, J. W.; Lee, H., Tannic Acid as a Degradable Mucoadhesive Compound. *ACS Biomaterials Science & Engineering* **2016,** *2* (4), 687-696.
106. Yan, W.; Shi, M.; Dong, C.; Liu, L.; Gao, C., Applications of tannic acid in membrane technologies: A review. *Advances in Colloid and Interface Science* **2020,** *284*, 102267.